Schizosphaerella size and abundance variations across the Toarcian Oceanic Anoxic Event in the Sogno Core (Lombardy Basin, Southern Alps)

Giulia Faucher*[1], Stefano Visentin [1], Gabriele Gambacorta [1] and Elisabetta Erba [1]

[1]*Department of Earth Sciences, Università degli Studi di Milano, 20133 Milan, Italy*

Email:
giulia.faucher@unimi.it
stefano.visentin@unimi.it
gabriele.gambacorta@guest.unimi.it
elisabetta.erba@unimi.it

Contact authors:
giulia.faucher@unimi.it

Abstract

Abundance and size variations of nannofossil *Schizosphaerella punctulata* were quantified in the uppermost Pliensbachian–Lower Toarcian succession recovered with the Sogno Core (Lombardy Basin, Northern Italy). High-resolution nannofossil biostratigraphy and C-isotopic chemostratigraphy identified the Jenkyns Event within the Toarcian oceanic anoxic event (T-OAE) interval. Absolute abundances and morphometric changes of "small *S. punctulata*" (< 7 µm), *S. punctulata* (7-10 µm; 10-14 µm; > 14 µm) and "encrusted *S. punctulata*" (specimens with a fringing crust) show large fluctuations across the negative $\delta^{13}C$ Jenkyns Event. The *Schizosphaerella* crisis is further characterized by a decrease in average valve size in the early–middle Jenkyns Event. The abundance fall was caused by the failure of *S. punctulata* specimens > 7 µm and "encrusted *S. punctulata*" that along with the increased relative abundance of small specimens, produced the reduction of average dimensions also documented in the Lusitanian and Paris Basins, although with a diachronous inception. The average valve size from the Lombardy Basin is ~2 µm smaller. Hyperthermal conditions associated with excess CO_2 and ocean acidification possibly forced the drastic reduction of *S. punctulata* abundance/size. In the pelagic succession of the Sogno Core there is a strong positive

correlation between the *S. punctulata* (> 7 µm) absolute abundance/size and the $CaCO_3$ content, with a negligible contribution by "small *S. punctulata*". Encrusted specimens testify selective neomorphic processes: the diagenetic crust seems diagnostic to separate *S. punctulata* from *S. astraea.*

Keywords: T-OAE; nannofossils; Jurassic; morphometry; calcareous nannoplankton

1. Introduction

The Toarcian oceanic anoxic event (T-OAE), dated as early Toarcian (*c.* 183 Ma; Early Jurassic), is considered one of the most extreme paleoenvironmental perturbations in Earth's history. It was characterized by global warming, accelerated weathering, sea level rise, oceanic anoxia and extensive accumulation of organic matter from coastal to pelagic settings (Jenkyns, 1985, 1988, 2010). The pelagic sedimentary successions archiving the T-OAE are key for the quantification and comprehension of the response of marine planktonic communities to the global perturbations that affected the ocean/atmosphere system. Since Triassic times (Bown, 1998; Bown et al., 2004; Erba, 2006; Gardin et al, 2012; Demangel et al., 2020) coccolithophores have been part of the primary producers responsible for energy transfer to higher trophic levels as well as export of organic matter and $CaCO_3$ from the photic zone to the deep ocean. Calcareous nannofossils include the fossil remains of coccolithophores, namely coccospheres and coccoliths as well as associated nannoliths often of unknown biological affinity such as *Schizosphaerella*. In Jurassic times, calcareous nannoplankton were already a most efficient rock-forming group (Erba, 2004, 2006) as testified by pelagic micrites essentially consisting of coccoliths and nannoliths, in addition to variable amounts of diagenetic calcite (Kälin, 1980; Kälin and Bernoulli, 1984). In particular, *Schizosphaerella,* a nannolith composed of two valves (Deflandre and Dangeard, 1938), can reach such high abundances (e.g. Kälin and Bernoulli, 1984; Claps et al., 1995; Mattioli, 1997; Erba, 2004; Casellato and Erba, 2015; Peti and Tibault, 2017) as to produce a "schizosphaerellite" (Erba et al. 2019a). In this work, we focus on *Schizosphaerella* across the T-OAE interval recovered in the Sogno Core that consists of pelagic,

well-dated (Visentin and Erba, 2021; Erba et al., 2022) limestones, marlstones and black shales from the Lombardy Basin (Figure 1).

More than a century ago, Dal Piaz (1907) in a pioneering and embryonic study for the paleoceanography of the Mesozoic, documented Toarcian organic-rich facies in Jurassic pelagic successions of the Southern Alps (Alpi Feltrine, Northern Italy) analogous to black shales in Germany and Switzerland (Posidonienschiefer), England (Jet Rock and Bituminous Shales) and France (Schistes Cartons). A few decades later, Gaetani and Poliani (1978) described a Lower Toarcian black shale interval named "*Livello a Pesci*" (Fish Level) in the pelagic succession of the Lombardy Basin (Figure 1).

Fig 1: about here, one and a half page

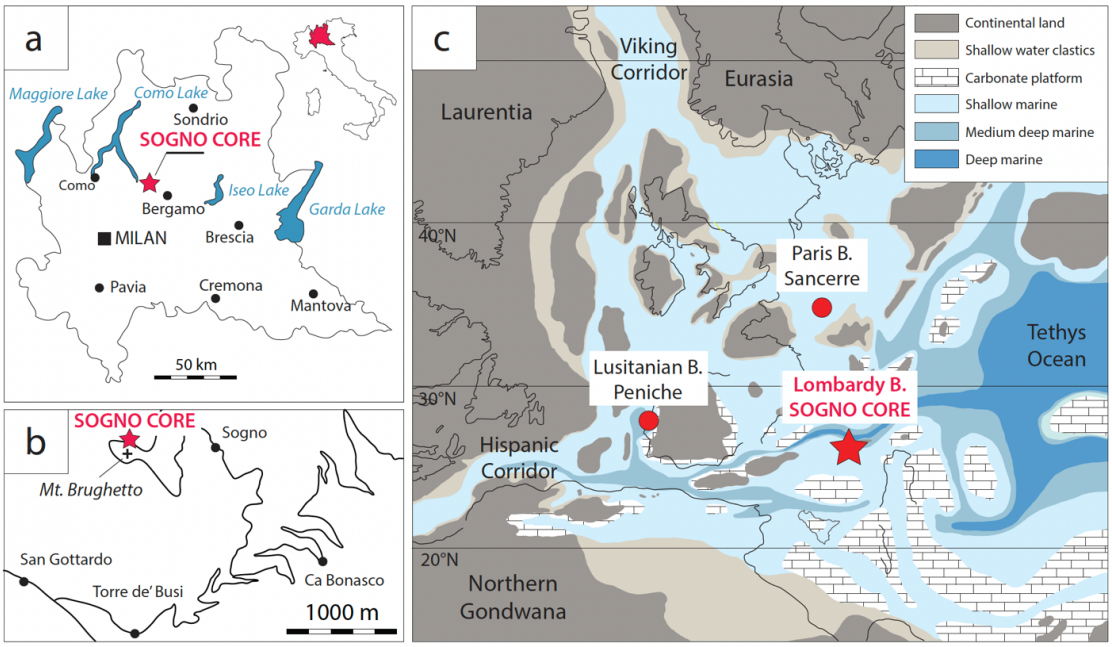

Figure 1. (a, b) Present-day location of the Sogno Core (modified after Erba et al., 2019b, 2022) (c) Paleogeographical map of western Tethys in the Toarcian (modified after Ruebsam et al., 2018) and paleo-location of the Sancerre–Couy borehole (Hermoso et al., 2009), Peniche (Hesselbo et al., 2007) and Sogno (this study).

The T-OAE was defined by Jenkyns (1985, 1988) on the basis of these coeval lithostratigraphic markers and soon later chemostratigraphic C- ~~and O-stable~~ isotopic investigations revealed a ubiquitous association of Lower Toarcian black shales with a major perturbation of the global carbon cycle, recorded by a positive anomaly of carbon-isotope curves obtained from sedimentary carbonate and/or organic matter (Jenkyns and Clayton, 1997; Jenkyns, 2003, 2010). The development of high-

resolution chemostratigraphy additionally identified a distinctive negative shift interrupting the broad T-OAE positive C isotopic excursions in terrestrial (lacustrine), shallow- and deep-marine archives (Jenkyns and Clayton, 1986; Hesselbo et al., 2000, 2007; Schouten et al., 2000; Röhl et al., 2001; Jenkyns et al., 2001, 2002; McElwain et al., 2002; Kemp et al., 2005; Emmanuel et al., 2006; van Breugel et al., 2006; Suan et al., 2008; Sabatino et al., 2009; Suan et al., 2010; Al-Suwaidi et al., 2010; Caruthers et al., 2011; Gröcke et al., 2011; Hesselbo and Pieńkowski, 2011; Kafousia et al., 2011, 2014; Izumi et al., 2012; Trabucho-Alexandre et al., 2012; Reolid, et al., 2014; Xu et al., 2017; Them et al., 2017; Fantasia et al., 2018; Ikeda et al., 2018; Filatova et al., 2020; Reolid et al., 2020; Ruebsam and Al-Husseini, 2020; Remirez and Algeo, 2020; Hougård et al., 2021).

Hougård et al. (2021) critically discussed the definition of the T-OAE that has been determined based on a variety of lithostratigraphic, geochemical and paleontological data, producing artefacts and/or misunderstandings in correlations and modelling at supra-regional scale. More recent studies renamed the T-OAE as the Jenkyns Event in which they distinguished the negative carbon isotope excursion (CIE, ~~their interval 2~~; Müller et al., 2017; Reolid et al., 2020). And recommended using the term Jenkyns Event for the global early Toarcian changes including anoxia, enhanced organic-matter burial, biotic crises in marine and terrestrial ecosystems, climate warming and sea-level rise. Yet, they did not provide a definition of the beginning and end of the Jenkyns Event, thus impeding its unequivocal identification for correlations at regional, supra-regional and global scale. Here, for our investigation, we applied the definition by Erba et al. (2022) that proposed naming as Jenkyns Event only the $\delta^{13}C$ negative anomaly within the T-OAE. Indeed, relatively detailed chemostratigraphic records through the T-OAE interval document that the Jenkyns Event comprises a lower part marked by a sharp decrease of the $\delta^{13}C$ curve followed by minimum values (isotopic segment Jenkyns 1 = J1), and an upper part corresponding to gradual recovery to pre-anomaly $\delta^{13}C$ values (isotopic segment Jenkyns 2 = J2) (Figure 2a). In the Sogno Core, the high resolution $\delta^{13}C$ chemostratigraphy allowed the recognition of the T-OAE positive excursion interrupted by the Jenkyns event negative shift (Figure 2).

The specific objective of this investigation is the quantification of changes in size and abundance of the micrite-forming schizosphaerellids to derive their biocalcification tempo and mode in response to the Jenkyns Event (J1 and J2) perturbation and also relative to the Fish Level black shale interval in the Sogno Core. The pelagic nature of the Sogno section (Gaetani and Poliani, 1978; Jenkyns and Clayton, 1986; Gaetani and Erba, 1990; Casellato and Erba, 2015; Erba et al., 2019b; Erba et al., 2022), deposited at ~ 1500 m water depth (Erba et al., 2022), is crucial for excluding the influence of shallow-water derived micrite and, thus, assessing the implications of *Schizosphaerella* biocalcification changes – in terms of abundance and size – for the pelagic carbonate sedimentation.

Fig 2: about here, full page width

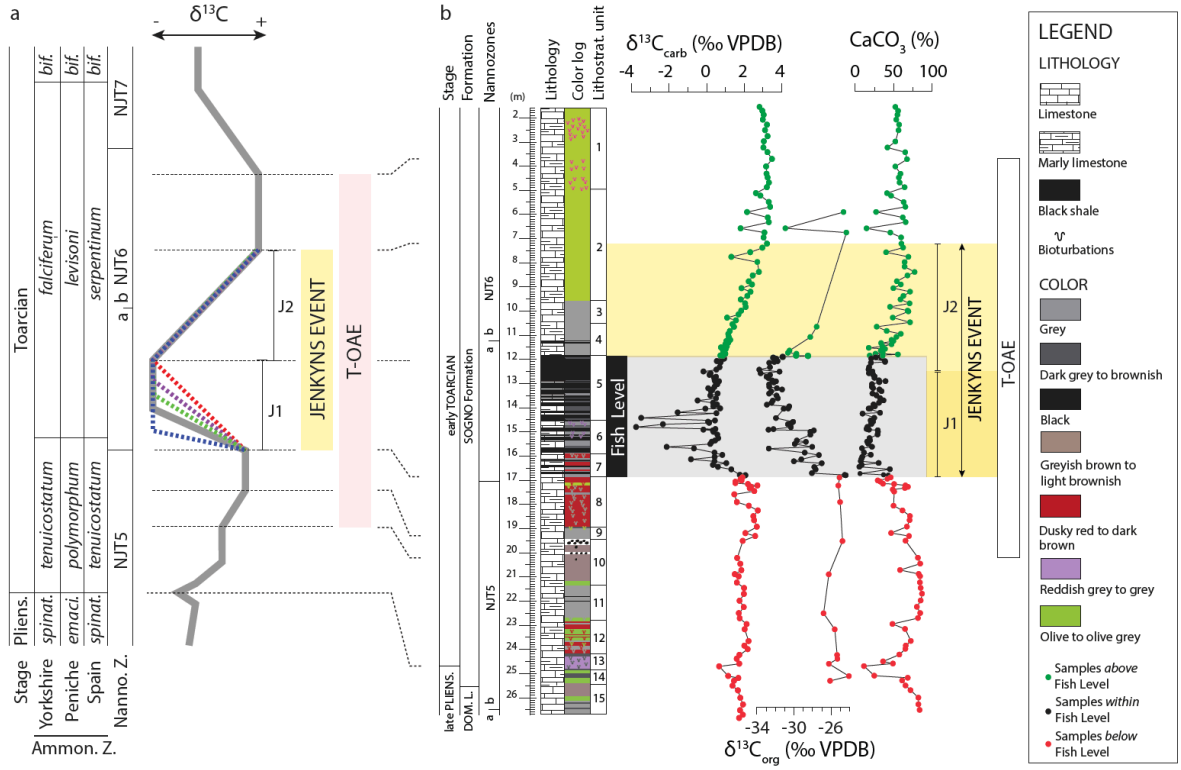

Figure 2. (a) Schematic $\delta^{13}C$ reference curve for the latest Pliensbachian–Toarcian time interval (modified after Ruebsam and Al-Husseini (2020), with minor modifications by Hougård et al. (2021)). The stratigraphic extent of the T-OAE (Jenkyns, 2010) is indicated with a light red rectangle, while the Jenkyns Event is indicated by a yellow band. Extent of the lower J1 and the upper J2 segments of the Jenkyns Event (Erba et al., 2022) are also illustrated. Coloured dashed lines in the reference plot represent the different trends documented in the lower part of the Jenkyns Event (J1). (b) Lithostratigraphy, isotopic records ($\delta^{13}C_{carb}$, $\delta^{13}C_{org}$) and $CaCO_3$ curve from Erba et al. (2019b, 2022). Nannofossil biostratigraphy from Visentin and Erba (2021).

Previous studies documented a temporary reduction in size for *Schizosphaerella* in the Upper Pliensbachian–Lower Toarcian interval (Mattioli and Pittet, 2002; Suan et al., 2008, 2010; Mattioli

et al., 2009; Reolid et al., 2014; Clémence et al., 2015; Peti and Thibaud, 2017; Erba et al., 2019a; Müller et al., 2020; Menini et al., 2021; Peti et al., 2021; see Supplementary Table S1). Moreover, a significant decline in schizosphaerellid abundance outlines the "*Schizosphaerella* crisis" starting just prior to the T-OAE black shale interval and representing the temporary breakdown of this rock-forming taxon (Claps et al., 1995; Erba, 2004; Tremolada et al., 2005; Casellato and Erba, 2015). Similar and coeval decreases in abundance of *Schizosphaerella punctulata* – and in general in nannofossil total abundances – are reported from various sections from western Tethys and the Boreal realm (Bucefalo Paliani et al., 2002; Mattioli et al., 2008; Mattioli et al., 2009; Fraguas et al., 2012, 2021; Hermoso et al., 2012; Clémence et al., 2015; Erba et al., 2015; Menini et al., 2021; Visentin et al., 2021) suggesting a major change in *Schizosphaerella* biocalcification at supra-regional scale. The comparison with similar datasets from various successions will be used to evaluate and separate local from regional/global adaptations and responses.

2. Materials and Methods

2.1 The Sogno core

The quantitative and morphometric analyses of *S. punctulata* were conducted on the Sogno Core drilled next to the outcrop on the northern slope of Monte Brughetto (Figure 1). Here a continuous pelagic sequence of Sinemurian to Kimmeridgian age was lithostratigraphically characterized and dated using bio-chemo-magneto-cyclostratigraphy (Gaetani and Poliani, 1978; Jenkyns and Clayton, 1986; Gaetani and Erba, 1990; Hinnov et al., 2000; Muttoni et al., 2005; Channell et al., 2010; Casellato and Erba, 2015). The outcropping strata were initially named Monte Brughetto section (Gaetani and Poliani, 1978; Jenkyns and Clayton, 1986) and later Colle di Sogno section (Gaetani and Erba, 1990; Hinnov et al., 2000; Muttoni et al., 2005; Channell et al., 2010; Casellato and Erba, 2015). This succession is pelagic, stratigraphically continuous and relatively expanded; it consists of limestone and marlstone, with chert and marly claystone as minor lithologies. At Colle di Sogno, in particular, the type-section of the Sogno Formation (Fm.) (Toarcian–earliest Bajocian) was formalized by Gaetani and Poliani (1978). Within the lower part of the Sogno Fm., the

~5 meter-thick interval of dark grey-to-black marly claystones is named Fish Level (Gaetani and Poliani, 1978; Gaetani and Erba, 1990; Casellato and Erba, 2015; Erba et al., 2022). In recent times, above the Upper Pliensbachian Domaro Limestone Fm., the Lower Toarcian portion of the Sogno Fm. results to be degraded by weathering and vegetation cover, especially as far as the Fish Level black shales are concerned. Therefore, a coring campaign was designed to obtain a continuous and well-preserved section across the Lower Toarcian and specifically the T-OAE stratigraphic record. The Sogno Core (45°47′20.5′′ N, 9°28′30.0′′ E) recovered 26.83 meters of continuous unweathered material (Erba et al., 2019b) that was characterized for lithostratigraphy (Erba et al., 2019b, 2022), calcareous nannofossil biostratigraphy (Visentin and Erba, 2021) and chemostratigraphy (Erba et al., 2022). Detailed sedimentological analysis allowed the identification of 15 lithostratigraphic units and a comprehensive characterization of the Fish Level (Erba et al., 2019b; 2022) (Figure 2b). Calcareous nannofossil semiquantitative analyses allowed to accomplish a high-resolution biostratigraphy of the latest Pliensbachian–early Toarcian time interval with the identification of the NJT 5 and NJT 6 Zones of the standard Tethyan nannofossil zonation (Mattioli and Erba, 1999), implemented due to the split of the NJT 6a and NJT 6b Subzones and the identification of the "*Schizosphaerella* crisis" and "*Schizospherella* recovery" (Visentin and Erba, 2021). The $\delta^{13}C$ – both on bulk carbonate and organic matter – chemostratigraphy of the Sogno Core provided a high-resolution record of the uppermost Pliensbachian–Lower Toarcian interval from the Lombardy Basin. Specifically, the Pliensbachian/Toarcian boundary is characterized by a minor negative anomaly followed by a broad positive excursion interrupted by the negative shift of the Jenkyns Event (Erba et al., 2022; Figure 2b).

2.2 Taxonomic notes for *Schizosphaerella punctulata*

The species *S. punctulata* was defined by Deflandre and Dangeard (1938) as a nannolith composed by two interlocked valves with a diameter of 12–30 µm. Later studies documented also definitively smaller specimens with valve width of 8–12 µm (Bown, 1987; Cobianchi, 1992) and 7–13.5 µm (Mattioli and Pittet, 2002). Casellato and Erba (2015) observed specimens even smaller than

7 µm that separated as "small *S. punctulata"*. Kälin (1980) described specimens of *S. punctulata* peculiarly bearing fringes of radial crystals in samples from the Southern Alps, Tuscany and Umbrian sequences. Similar features were later reported from Jurassic deep-water calcareous sediments from the Mazagan Plateau off Morocco at Deep Sea Drilling Project (DSDP) Hole 547B and demonstrated to be of early diagenetic origin producing neomorphic calcite, seemingly related to low Mg/Ca ratios of oceanic and consequently interstitial waters (Kälin and Bernoulli, 1984). Within genus *Schizosphaerella*, the species *S. astraea* was established by Moshkovitz (1979) as a nannolith with two hemispherical valves attached one to the other by a simple overlapping. The outer and inner valves have a diameter of respectively 16 and 14 µm. Moshkovitz (1979) specified that *S. astraea* differs from *S. punctulata* for the wall ultrastructure consisting of elongated crystals of 0.3-0.5 µm that are radiating from a central knob and forming a star-like pattern. The ultrastructure patterns of *S. punctulata* and *S. astraea* were further characterized in detail by Kälin and Bernoulli (1984) who demonstrated that diagenesis produces different modifications based on the original wall ultrastructure.

Schizosphaerella punctulata specimens with a fringing crust were observed in the uppermost Pliensbachian–Lower Toarcian interval at Colle di Sogno by Casellato and Erba (2015) who, thus, separated an "encrusted *S. punctulata*" morphogroup (Figure 3).

187 *Fig 3: about here, full page width*

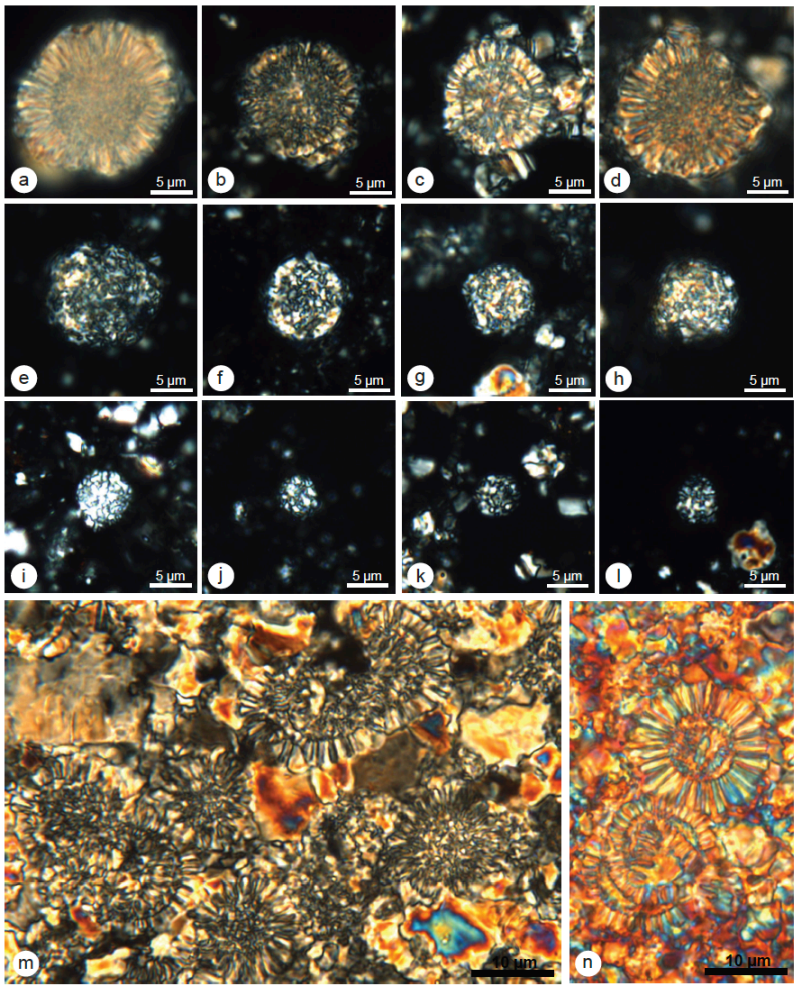

188 **Figure 3.** *Schizosphaerella* specimens from the Sogno Core photographed with the light polarizing microscope:
189 micrographs a-l belong to settling slides whereas m-n to ultrathin sections. a-d: "encrusted *S. punctulata*", cross-
190 polarized light; (a) sample S3 C12 330 (17.16 m), (b) sample S3 C18 385 (20.98 m), (c) sample S3 C19 397 (21.70
191 m), (d) sample S3 C28 450 (25.17 m); e-h: *S. punctulata*, cross-polarized light; (e) sample S3 C10 322h (15.86 m),
192 (f) sample S3 C7 320a (14.68 m), (g) sample S3 C18 385 (20.98 m), (h) sample S3 C4 309a (12.87 m); i-l: "small
193 *S. punctulata*", cross polarized light; (i) sample S3 C3 306 (12.51 m), (j) sample S3 C11 323 (16.78 m), (k) sample
194 S3 C15 361 (18.92 m), (l) sample S1 C31 184 (11.57 m); m: "encrusted *S. punctulata*" and *S. punctulata* specimens
195 from the lowermost Sogno Fm. unit 11, cross polarized light; sample S3 C19 397 (21.7 m); n: "encrusted *S.*
196 *punctulata*" specimens from the lowermost Sogno Fm. unit 12, quartz lamina, sample S3 C23 434 (23.98 m).

197 ### 2.3 Quantification of *Schizosphaerella punctulata* sizes and absolute abundances

198 A total of 46 samples from the Sogno Core were investigated for morphometric analyses of *S.*
199 *punctulata.* For each sample smear slides were prepared using the random settling technique (Geisen
200 et al., 1999). Morphometric analyses were conducted on 50 specimens of *S. punctulata* and 30
201 additional specimens of "encrusted *S. punctulata*", when present. All specimens were digitally
202 photographed in random fields of view using a Q-imaging Micro publisher 5.0 RTV camera mounted

on a Leitz Laborlux optical polarizing light microscope at 1250X magnification and a PC with Q-capture Pro suite software adapted for nannofossil analyses. Measurements were taken using ImageJ software, with an error of measurements of ± 0.08 µm. Given the structure of *S. punctulata*, the valve width, *sensu* Clémence et al. (2015), was measured (Figure 4). For specimens of "encrusted *S. punctulata*", in addition to the valve width, the thickness of the crust was measured.

After the construction of the dataset (measurements of 2690 *S. punctulata* specimens as detailed in Supplementary Table S2 and in the research data files), the size and abundance trends were considered subdividing *S. punctulata* into classes following two different approaches:

1) *sensu* Peti et al. (2021) who determined three *S. punctulata* size groups: S (small < 10 µm); M (medium > 9 µm and < 14 µm) and L (large > 14 µm). However, since the values indicated by Peti et al. (2021) for the S and M classes partly overlap, we allocated to the M group the specimens with a 10-14 µm size;

2) *sensu* Casellato and Erba (2015) who separated "small *S. punctulata*" (< 7 µm), *S. punctulata* (> 7 µm) and "encrusted *S. punctulata*".

Fig 4: about here, half page

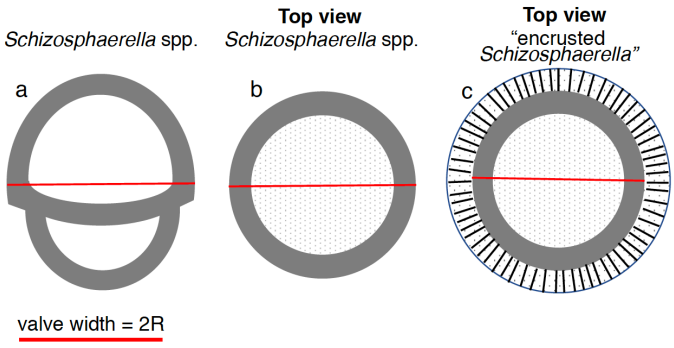

Figure 4. Schematic structure of *Schizosphaerella* and measurement simulations; a) two joint valves that form the entire individuals of *Schizosphaerella* spp. b) *Schizosphaerella* spp. top view; c) top view of "encrusted *Schizosphaerella punctulata*".

Following Casellato and Erba (2015) absolute abundances were gained counting all *S. punctulata* specimens in 1 mm^2 of ultrathin sections (7 µm-thick), separating specimens of *S. punctulata* (> 7 µm), "small *S. punctulata"* (< 7 µm) and "encrusted *S. punctulata*". These absolute

abundance analyses were performed on a selected number of sample (23 samples) encompassing the interval before, during and after the Fish Level. The ultrathin sections sampled variously oriented specimens of *Schizosphaerella* and cut individual valve potentially at different heights, thus the values obtained could be (partially) undermined. However, the full congruity of the results gathered with the ultrathin sections and those obtained with smear slides (Casellato and Erba, 2015; this study) indicates that the ultrathin section measurements reflect real trends.

The volume of *Schizosphaerella* was also inferred from the measured width valve values (Figure 4). The volume was calculated as (1):

$$Volume\ of\ one\ valve\ = ((\frac{4}{3}\pi(R^3 - \left(\frac{2}{3}R\right)^3)0.7)/2 \quad (1)$$

where R is half of the valve width. The valves of *Schizosphaerella* consist of calcite crystals with a considerable but variable primary porosity. For our calculations, we considered 30% porosity following Mattioli and Pittet (2002).

The volumes were used to estimate the grams of $CaCO_3$ produced by a single specimen of *Schizosphaerella* (2):

$CaCO_{3\ Schizo}$ = Volume *Schizosphaerella* * absolute abundances * density of calcite (2)

Statistical parameters like mean, median, standard deviation and 90% confidence level were calculated using the Matlab and PAST softwares and reported in Table 1. The complete set of measurements is available in the Supplementary files and in the research data files.

3. Results

3.1 Evolution of *Schizosphaerella* spp. size

In the investigated interval, the average valve size of *S. punctulata* is 8.49 µm, with variations from a minimum of 3.53 µm to a maximum value of 21.15 µm (Figure 5, Table 1). In the lower part of the Sogno Core (uppermost Pliensbachian–lowermost Toarcian, from 26.83 m to 21.70 m),

Schizosphaerella average sizes fluctuate between 8.70 and 9.97 µm with no appreciable changes passing from the Domaro Limestone Fm. to the Sogno Fm. A sharp decrease in size down to an average of 7.51 µm is observed across the Fish Level whose base correlates with the onset of the Jenkyns Event (Figure 5 and Table 1). An increase in *Schizosphaerella* valve size occurs just above the Fish Level starting in the lowermost part of the J2 segment of the Jenkyns Event where the average values are ~8.31 µm. A maximum average value of 9.81 µm was observed just above the top of the Jenkyns Event (at 6.76 m) followed by a *Schizosphaerella* size return to average values of 8.09 µm in the uppermost part of the Sogno Core.

Fig.5: about here, one and a half page

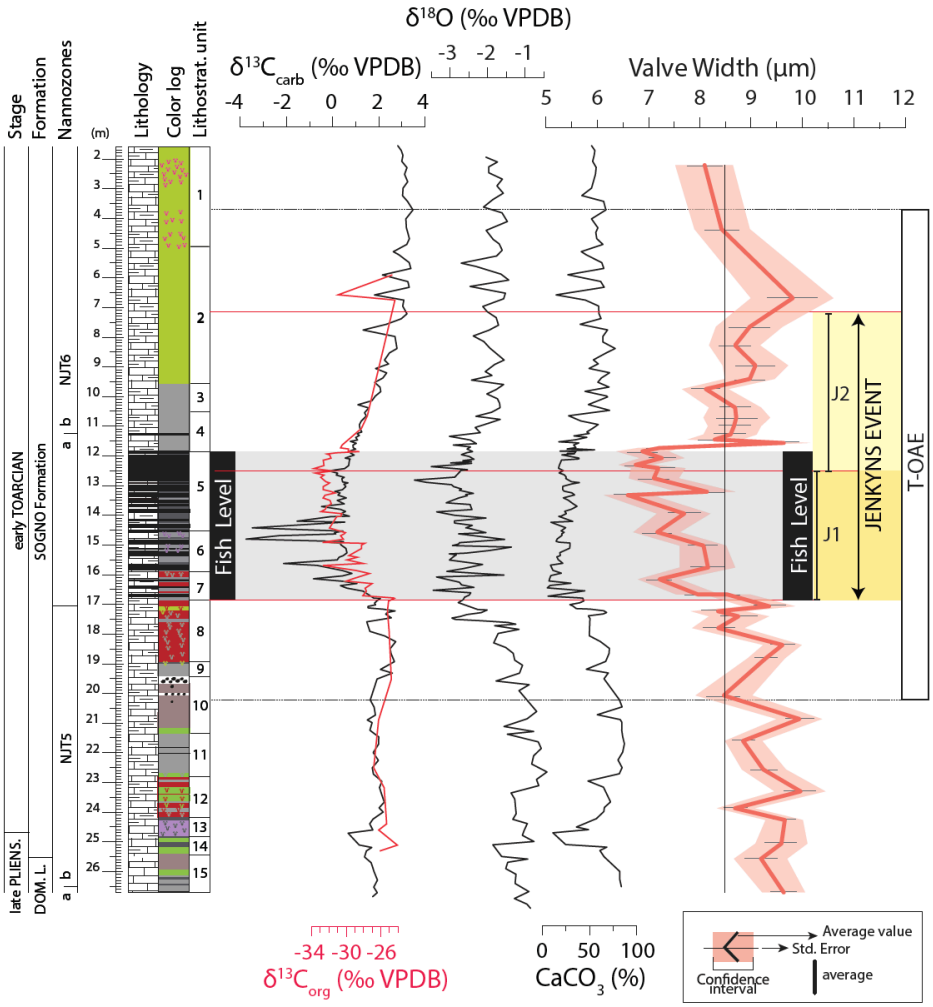

Figure 5. Uppermost Pliensbachian to Lower Toarcian *Schizosphaerella punctulata* size variations from the Sogno Core. The mean valve width variation of the overall *S. punctulata* population, the confidence interval (90%) and the sd. error are given. The grey band highlights the Fish Level. Extent of the T-OAE, the lower J1 and the upper J2 segments of the Jenkyns Event are also illustrated. Lithostratigraphy, isotopic records ($\delta^{13}C_{carb}$, $\delta^{13}C_{org}$, $\delta^{18}O$) and $CaCO_3$ from Erba et al. (2019b, 2022).

Broadly speaking, the first reduction in valve size from ~9 µm (in the pre-Fish Level interval) to ~7.5 µm (in the Fish Level) parallels the decrease in $CaCO_3$ content from ~ > 72% to < 26% and, similarly, the increase in *Schizosphaerella* size recorded in the J2 part of the Jenkyns Event correlates with a progressive increase in $CaCO_3$ content (Figure 5). Figure 6 illustrates the Pearson correlation coefficient of *S. punctulata* valve average width and the $CaCO_3$ %: a positive relationship is documented by a coefficient r = 0.71.

	W Average	st.dev	Min.	Max.	V Average	st.dev	Min.	Max.
J2	8.31	0.88	3.81	17.37	179.45	52.76	10.66	762.34
J1	7.69	0.59	3.53	16.29	138.48	29.27	10.94	589.54
post Fish Level	8.77	0.51	4.02	18.28	211.11	43.81	16.18	925.35
Fish Level	7.51	0.59	3.53	16.29	129.64	29.66	10.66	574.58
pre Fish Level	9.16	0.53	3.66	21.15	230.66	39.43	12.19	1080.48

Table 1. Average sizes of *S. punctulata* (all measurements) in the analyzed intervals. W average = average valve width, in µm; st.dev = standard deviation. Min. = minimum value; Max. = maximum value; V average = average volume in μm^3

Fig.6: about here, half page

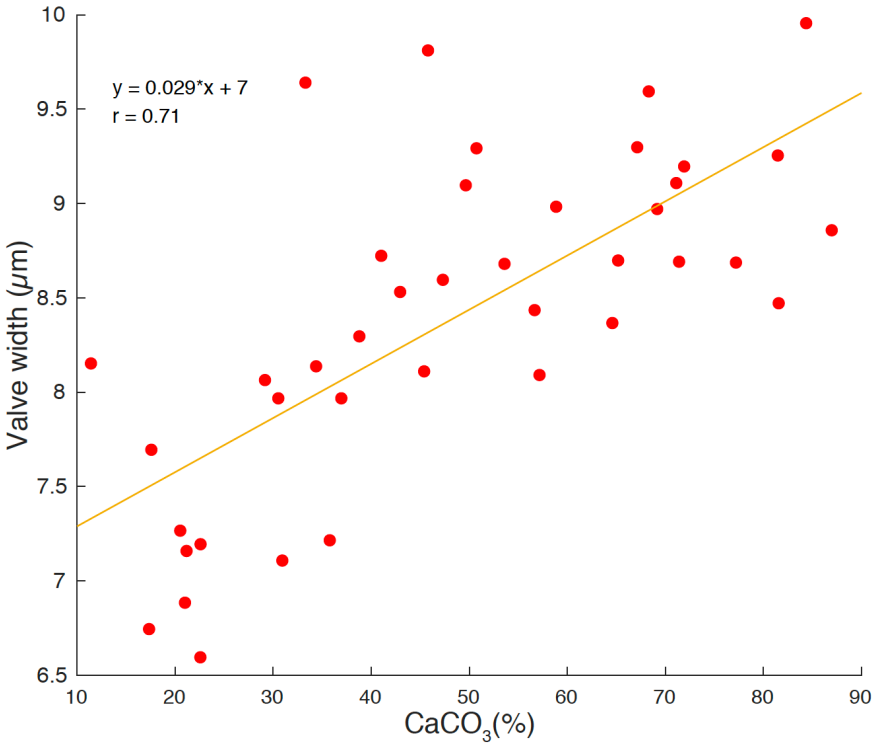

Figure 6. Scatter plot of the variations of $CaCO_3$ (%) versus the average valve width (µm). N = 46. The p value is < 0.05 for the correlation.

Following Peti et al. (2021) we separated *S. punctulata* into three groups characterized by specific valve sizes (S, M and L) that evidence different trends through the analyzed interval (Figure 7). The S group shows a reduction in average size in the Fish Level (from 7.96 µm before the Fish

Level to 6.92 µm in the Fish Level; supplementary Table S3) and a subsequent size increase (average of 7.56 µm) without, however, reaching the values of the pre-Fish Level interval. Specimens of the M group don't show any size trend with the exception of a transient increase in the valve size above the Fish Level where the valves reach 13.97 µm at 11.38 meter (sample S1C30 #180). The L group is extremely rare and sparse. In particular, specimens > 14 µm are absent in a few samples within the Fish Level. The L group does not show size trends through the analyzed interval.

We quantified the variations in relative abundance (percentage) of the three size-groups (Figure 7): in the Fish Level there is a slight increase in the percentage of specimens < 10 µm passing from 67 to 88%. This variety is the most represented in the whole assemblage and, thus, seems to control the trends obtained for the average valve sizes.

Fig.7: about here, full page

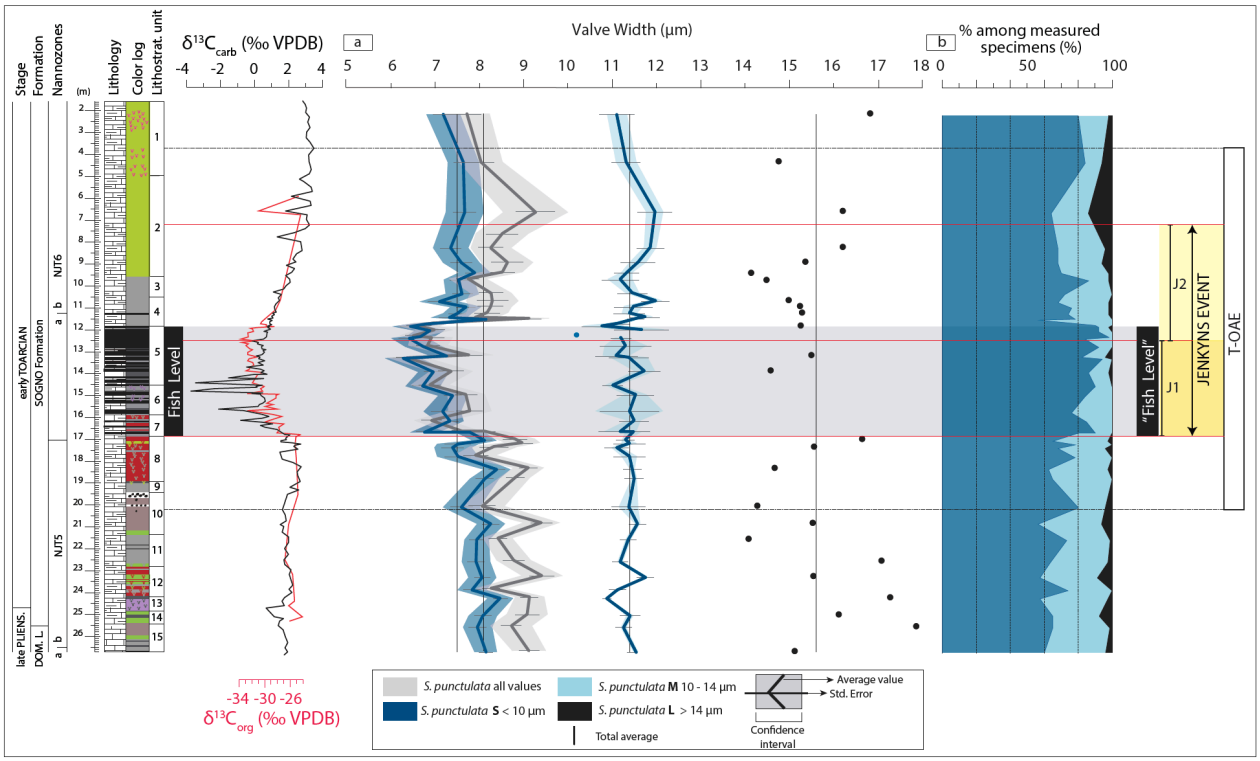

Figure 7. (a) Uppermost Pliensbachian to Lower Toarcian *S. punctulata* size variations using the varieties of Peti et al. (2021) of *S. punctulata:* S (< 10 µm), M (10 – 14 µm), and L (> 14 µm). The values of the L group are represented as dots since in some samples only one specimen is bigger than 14 µm and, therefore, the std. deviation and confidence interval cannot be calculated. (b) Percentage (%) of S (< 10 µm), M (10-14 µm), and L (> 14 µm).

We also subdivided our data following the categories of Casellato and Erba (2015), separating "small *S. punctulata"* (valve size < 7 µm), *S. punctulata* (valve size > 7 µm) and "encrusted *S. punctulata"* (all specimens characterized by a crust surrounding the valve). For the latter, the size refers only to the valve width independently from the crust thickness. The size variations of the three morphogroups are represented separately in Figure 8 and Table 2.

Fig.8: about here, full page width

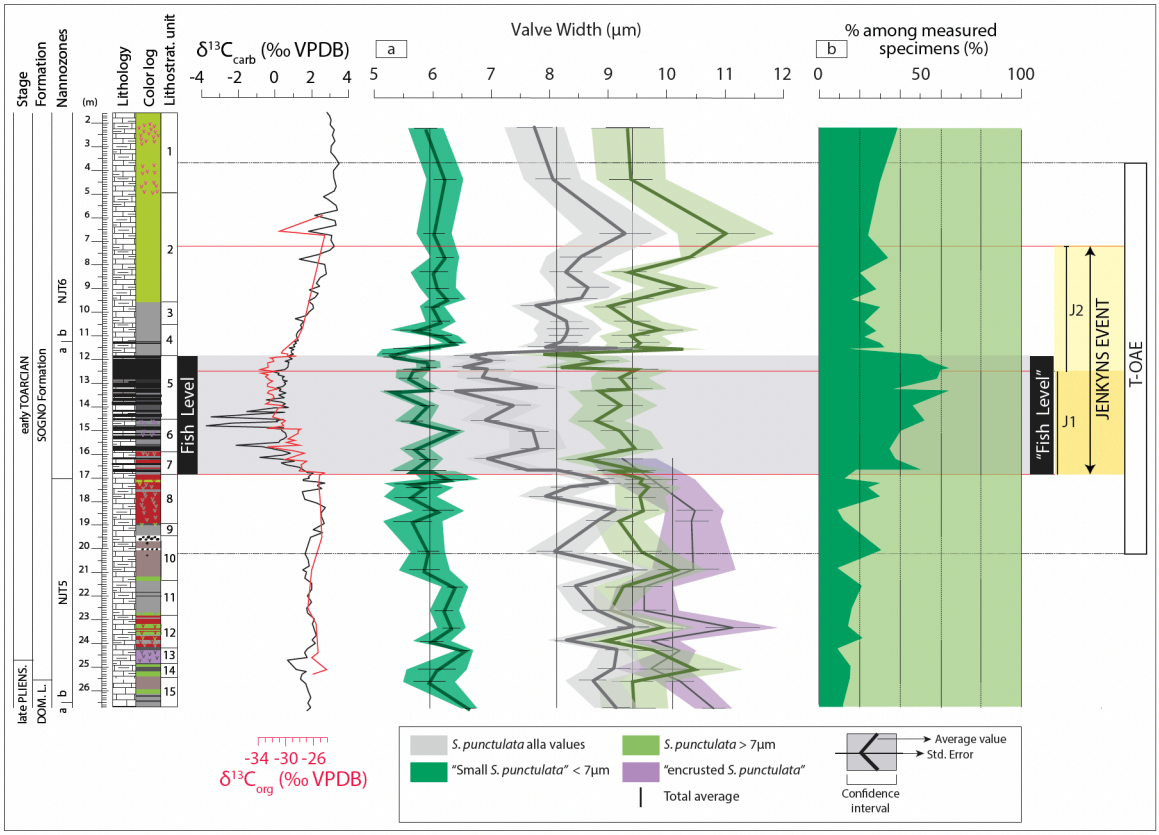

Figure 8. (a) Uppermost Pliensbachian to Lower Toarcian *S.punctulata* size variations using the groups of Casellato and Erba (2015): "small *S. punctulata"* (< 7 µm), *S. punctulata* (> 7 µm), and "encrusted *S. punctulata"*; (b) Percentage (%) of "small *S. punctulata"* (< 7 µm) versus *S. punctulata* (> 7 µm) + "encrusted *S. punctulata.*

	"small *S. punctulata"*		*S. punctulata* > 7µm		"encrusted *S. punctulata*"	
	W Average	st. dev	W Average	st. dev.	W Average	sd.dev
J2	5.93	0.32	9.33	0.74		
J1	5.79	0.28	9.16	0.31		
post Fish Level	6.04	0.21	9.73	0.55		
Fish Level	5.75	0.29	8.95	0.49	9.24	NA
pre Fish Level	6.06	0.31	9.57	0.39	10.10	0.42

Table 2. Average valve sizes of *S.punctulata* split by morphogroups of Casellato and Erba, (2015): "small *S. punctulata"* (< 7 µm), *S. punctulata* (> 7 µm), and "encrusted *S. punctulata"* in the analyzed interval. W average = average valve width, in µm; st.dev = standard deviation.

306 Specimens of *S. punctulata* > 7 µm show a size trend similar – but not identical – to the one
307 derived for average values (Figure 5) since a reduction in size from an average of 9.57 µm to an
308 average of 8.95 µm occurs within the Fish Level (Table 2). The minimum values of *S. punctulata* (>
309 7 µm) valve size were detected in the topmost part of the Fish Level (average 7.89 µm, at 11.86 m).
310 Specimens of "encrusted *S. punctulata*" occur only in the lower interval of the Sogno Core, namely
311 in the Domaro Limestone Fm. and the lowermost part of the Sogno Fm. below the Fish Level; this
312 morphogroup is extremely rare in the basal part of the black shale interval and absent from 16.29 m
313 upwards. The average valve size of "encrusted *S. punctulata*" specimens is slightly bigger (~10 µm)
314 compared to the *S. punctulata* specimens > 7 µm (average 9.42 µm) (Figure 8a). A relative decrease
315 in "encrusted *S. punctulata*" valve size precedes the Fish Level, reaching a minimum value (9.2 µm)
316 in the lowermost sample of the black shale interval (Figure 8a). As far as the thickness of the crust is
317 concerned, our data show no correlation with the dimension of the "encrusted *S. punctulata*" valve (r
318 = 0.018 see Supplementary Figure S1).

319 The valve size of "small *S. punctulata*" is 5.95 µm on average and shows modest fluctuations through
320 the investigated interval, from 16.79 to 11.86 m. The smallest values of 5.33 and 5.30 µm were
321 recorded within the Fish Level at 13.42 m (sample S3C5#313) and 11.86 m (sample S1C32#192),
322 respectively. It is worth noting that specimens of the "small *S. punctulata*" morphogroup display a
323 valve width ~2 µm smaller than *S. punctulata* (> 7 µm) (Figure 8a). The relative abundances of the
324 "small *S. punctulata*" (< 7 µm) and *S. punctulata* (> 7 µm) specimens vary through the studied
325 interval (Figure 8b). Indeed, the percentage of "small *S. punctulata"* (< 7 µm) substantially increases
326 in the Fish Level, passing from ~20% to 40-60% and returning to 20-30 % in the overlying interval
327 (Figure 8b).

328 Figure 9 illustrates the average size variations obtained for the following groups: specimens <
329 7 µm, specimens 7-10 µm, specimens 10-14 µm, specimens > 14 µm. Interestingly, the average values
330 are rather stable in individual curves, with only a negligible decrease in size across the Fish Level.

The relative abundances of these groups (Figure 9b) evidence a major increase in percentages of the specimens < 7 µm while the other size-groups display a decrease of variable amplitude. In fact, the 7-10 µm group passes from 49% to 40 % from the pre-Fish Level interval to the Fish Level interval. The 10-14 µm specimens show a more pronounced decrease from 30% to 12 %, and the > 14 µm group remains very rare with percentages between 1 and 3 %. The average size of "encrusted *S. punctulata*" is also reported in Figure 9a: this category pertains to specimens of average size comprised between 9.2 and 10.8 µm, and falls between the curves of the size-groups 7-10 µm and 10-14 µm.

Fig.9: about here, full page width

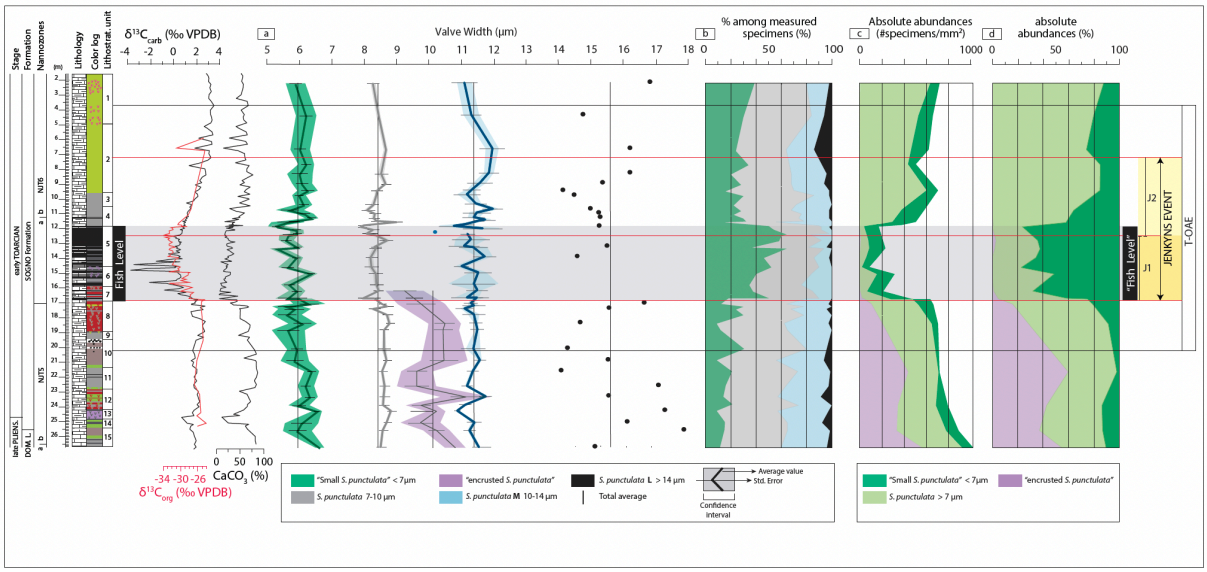

Figure 9. Uppermost Pliensbachian to Lower Toarcian *S. punctulata* size variations. (a) Valve width variations split by varieties *sensu* Casellato and Erba, (2015) and Peti et al. (2021): "small *S. punctulata"* (< 7 µm), "encrusted *S. punctulata"*, variety S p.p. (7-10 µm), M (10 - 14 µm) and L (>14 µm); (b) relative abundances: percentage (%) of "small *S. punctulata"* (< 7 µm), variety S p.p. (7 - 10 µm), M (10 - 14 µm) and L (>14 µm; (c) absolute abundances of "small *S. punctulata"* (< 7 µm), *S. punctulata* (> 7 µm), "encrusted *S. punctulata"*; (d) absolute abundance percentages (%) of "small *S. punctulata"* (< 7 µm), *S. punctulata* (> 7 µm) and "encrusted *S. punctulata"*.

3.2 Evolution of the abundances of the *Schizosphaerella* morphogroups

Based on the relative abundances of the size-groups determined following both Peti et al. (2020) and Casellato and Erba (2015), it is evident that specimens < 7 µm show the greatest variations in percentages. Consequently, we evaluated the absolute abundances (number of specimens) of "small *S. punctulata*" (< 7 µm) versus *S. punctulata* (> 7 µm) and "encrusted *S. punctulata*" in 1 mm^2 of ultrathin sections (Figure 9c; Supplementary Table S4). The absolute abundances (Figure 9c) of total

352 *Schizosphaerella* (*S. punctulata* (> 7 μm) + "small *S. punctulata"* (< 7 μm) + "encrusted *S.*
353 *punctulata"*) is highest in the Domaro Limestone Fm. (~1000 specimens/mm^2) and slightly decreases
354 in the lower part of the Sogno Fm. (~700 specimens/mm^2). In the Fish Level the *Schizosphaerella*
355 absolute abundance drops to the lowermost value of 89 specimens/mm^2 (average of ~290
356 specimens/mm^2) and returns to ~600 specimens/mm^2 in the overlying section.
357 In the uppermost Pliensbachian-lowermost Toarcian interval the numbers of "encrusted *S.*
358 *punctulata"* first decrease passing from the Domaro Limestone Fm. (~500 specimens/mm^2) to the
359 Sogno Fm. (~ 300 specimens/mm^2) and then progressively decline starting below the Fish Level
360 within which no specimens have been observed, similarly to the interval overlying the black shales.
361 The absolute abundance of *S. punctulata* specimens > 7 μm remains stable from the lowermost sample
362 up to the base of the Fish Level (~380 specimens/mm^2) and suddenly decreases within the black shale
363 interval. In the lower and upper parts of the Sogno Core, the "small *S. punctulata*" (< 7 μm)
364 morphogroup displays absolute abundances of 140-150 specimens/mm^2 and only one sample within
365 the Fish Level records a low abundance value (69 specimens/mm^2, sample S3C7 #320a, 15.11 m;
366 Figure 9c). Percentages of *S. punctulata* (> 7 μm), "small *S. punctulata"* (< 7 μm) and "encrusted *S.*
367 *punctulata"* specimens were derived from their absolute abundances as illustrated in Figure 9d.
368 Again, within the Fish Level the "small *S. punctulata"* (< 7 μm) specimens become dominant (>
369 60%) similarly to what observed for the proportions derived from the set of measured specimens
370 (Figure 8b). Thus, the latter are not an artifact to be ascribed to the "close sum problem", but, indeed,
371 reflect major changes in absolute abundances of "small *S. punctulata"* (< 7 μm) versus *S. punctulata*
372 specimens > 7 μm. At the same time, the consistency of the relative abundances derived from the
373 dimensional dataset and from the absolute abundances suggests that the latter are not affected by the
374 cutting/orientation of the ultrathin sections.
375 The switch in relative and absolute abundances of the *S. punctulata* size-groups explains the
376 sharp decrease in average *S. punctulata* valve size across the Fish Level (Figure 5): specifically, the

377 average size decrease is not the result of a general valve reduction, but rather derives from the drop
378 in abundance of *S. punctulata* specimens > 7 µm.

379 **3.3 The contribution of *S. punctulata* to the pelagic micrites of the Sogno Core.**

380 Investigation of ultrathin sections allows the quantification in a unit area (1 mm^2 in our case)
381 of the absolute abundance of individual nannofossil taxa (e.g., Erba and Tremolada, 2004). As
382 previously documented for the Colle di Sogno section (Casellato and Erba, 2015), in the Sogno Core
383 large amounts of the micrite consists of schizospaherellids (Figure 3m). Based on the equation
384 proposed by Mattioli and Pittet (2002) (equations 1 in XXXXX) and our equation 2, we calculated
385 the volume and mass of *S. punctulata* (> 7 µm) and "small *S. punctulata*" (< 7 µm) specimens. As
386 expected, the variations in *S. punctulata* calcite (= mass) are strictly related to the absolute
387 abundances and this is true for the whole *S. punctulata* dataset as well as for individual morphogroups
388 (Figure 9c,d). In fact, the "small *S. punctulata*" (< 7 µm) calcite remains low (between 0.02 and 0.34
389 10^{-7} g) whereas the amount of calcite produced by *S. punctulata* specimens > 7 µm (with and without
390 fringing crust) is highest in the Domaro Limestone Fm. (7.1 10^{-7} g), sharply decreases (4.6 10^{-7} g) in
391 the Sogno Fm. below the Fish Level where minimum values around 0.1 10^{-7} gr were observed before
392 returning to an average of 3.6 10^{-7} g (Figure 10). It is also evident that the total calcite produced by
393 *S. punctulata* substantially derive from specimens > 7 µm with a very minor contribution by
394 specimens < 7 µm (Figure 10).

Fig.10: about here, one and a half page

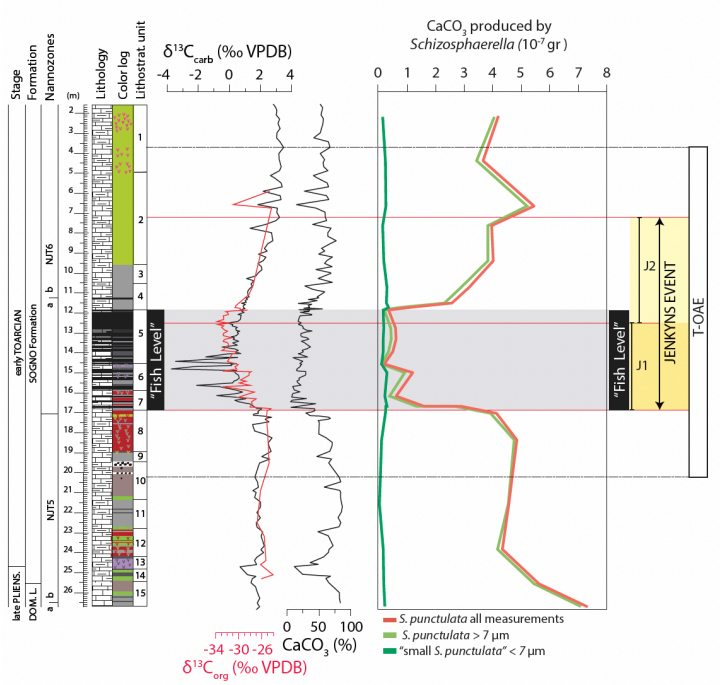

Figure 10. Grams of calcium carbonate produced by *Schizosphaerella punctulata* (all measurements), *S. punctulata* (> 7 µm) and "small *S. punctulata"* (< 7 µm).

Since schizosphaerellids are rock-forming, we evaluated their patterns of absolute abundance, size and mass relative to the $CaCO_3$ content, considering both the total S. *punctulata* cluster and the two morphogroups < 7 µm and > 7 µm separately (Figure 11). A very high Pearson coefficient was found between the calcium carbonate content and total calcite produced by the *S. punctulata* cluster (r = 0.89; Figure 10a) as well as between the calcium carbonate content and total absolute abundance of all *S. punctulata* specimens (r = 0.88; Figure 10b). However, this is due to specimens > 7 µm (Figure 10c) because no correlation has been extracted for the correlation between the $CaCO_3$ content and the "small *S. punctulata"* (< 7 µm) absolute abundance (r = -0.52; Figure 10b) or calcite (r = -0.34; Figure 10c). We further assessed the influence of the valve size on the calcium carbonate content and concluded that, again, changes in the "small *S. punctulata*" (< 7 µm) dimensions are irrelevant (r= 0.47; Figure 10d), but a positive correlation links specimens > 7 µm to the $CaCO_3$ amount (r = 0.73; Figure 10d).

Fig.11: about here, one and a half page

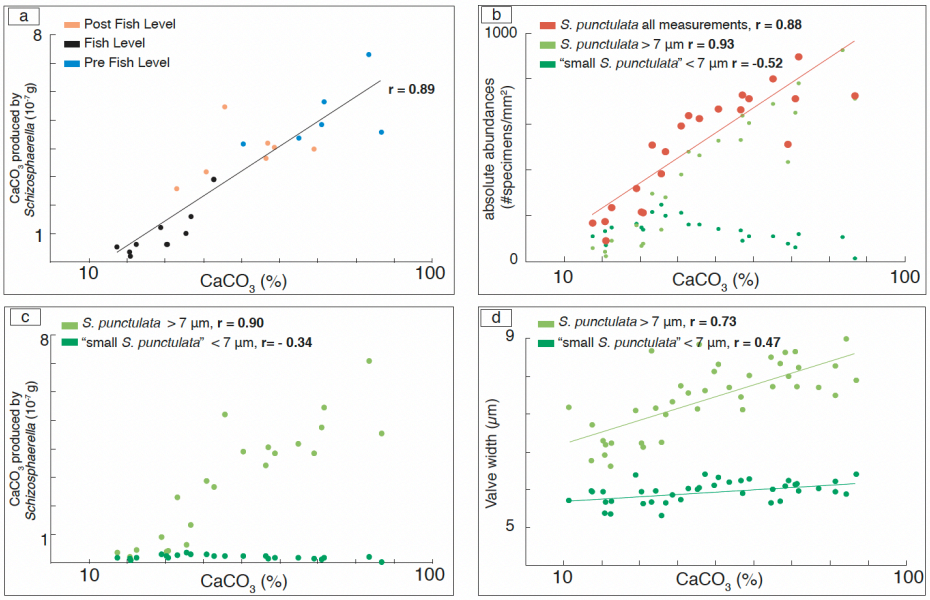

Figure 11. Scatter plots of the variations of $CaCO_3$ (%) versus: (a) grams of calcium carbonate produced by *S. punctulata* (all measurements) through three different intervals (pre-Fish Level, Fish Level, post-Fish Level), (b) absolute abundances of *S. punctulata* (> 7 µm), "small *S. punctulata*" (< 7 µm) and "encrusted *S. punctulata*"; (c) grams of calcium carbonate produced by *S. punctulata* (> 7 µm) and "small *S. punctulata*" (< 7 µm); (d) valve width (µm) of *S. punctulata* (> 7 µm) and "small *S. punctulata*" (< 7 µm). The p values are < 0.05 for all the correlations.

4. Discussion

4.1 Comparison with previous studies

The characterization of abundance and size of *S. punctulata* in Lower Jurassic successions from western Tethys (Claps et al., 1995; Mattioli and Pittet, 2002; Erba 2004; Suan et al., 2008, 2010; Mattioli et al., 2009; Reolid et al., 2014, 2021; Erba et al., 2019a; Muller et al., 2020) and the Boreal Realm (Clémence et al., 2015; Peti and Thibault, 2017; Menini et al., 2021; Peti et al., 2021) documented significant changes associated to the T-OAE and specifically the negative $\delta^{13}C$ Jenkyns Event. There is a general consensus on the litho-biogenetic role, during the Early Jurassic, of schizosphaerellids which in fact produced most of the pelagic carbonate with minor contributions by other coccoliths and nannoliths (e.g. Mattioli and Pittet, 2002; Erba, 2004; Suan et al., 2008, 2010). This pattern was interrupted during the Jenkyns Event as evidenced by a significant decline in abundance of *S. punctulata*, becoming negligible as micrite-forming component. The record from the Sogno Core (Figures 5 and 9) is fully consistent with previous datasets and indicate that locally the *Schizosphaerella* crisis interval corresponds to the Fish Level as previously documented by Casellato and Erba (2015) for the Colle di Sogno outcrop. This bio-lithostratigraphic coincidence suggests that the abundance decline of *S. punctulata* is closely linked to black shale deposition. However, this is not a general rule, since black shales are not synchronous at regional to supra-regional scale (e.g.

433 Erba et al., 2022). Therefore, surface (nannofossil assemblages) and bottom (oxygen depletion) water
434 changes were not synchronous, even within the same depositional basin. As far as the perturbation of
435 the C-cycle is concerned, the high-resolution C-isotopic chemostratigraphy of the Sogno Core
436 unambiguously indicates that the onset of the *Schizosphaerella* crisis correlates with the sharp initial
437 decrease of the Jenkyns Event negative anomaly, while the *Schizosphaerella* recovery phase
438 commences in the lowermost part – although not at the base – of the J2 segment (Figure 9c).
439 Morphometric investigations of *Schizosphaerella* valves in Lower Jurassic successions
440 (Mattioli and Pittet, 2002; Suan et al., 2008, 2010; Reolid et al., 2014; Erba et al., 2019a) revealed
441 fluctuations in size with potential causal relationships with altered biocalcification during times of
442 perturbed oceanic chemistry. Figure 12 illustrates the fluctuations in *Schizosphaerella* valve size
443 quantified relative to high-resolution chemostratigraphy in the Paris Basin (Sancerre section, Peti and
444 Thibault, 2017) and Lusitanian Basin (Peniche section, Suan et al., 2010) compared to the Sogno
445 Core record. *Schizosphaerella* reduction in size results to be broadly correlatable in separate basins
446 pointing to a common cause, rather than local depositional oceanographic regimes, regardless of the
447 presence/absence of black shales and their distribution with respect to C stable isotopes. However,
448 while the return to larger valves appears synchronous in the early phase of the J2 segment, the
449 inception of reduced dimensions is diachronous: the decline in *Schizosphaerella* valve size started
450 well before the onset of the negative $\delta^{13}C$ shift at Sancerre, whereas it was slightly older than, and
451 synchronous with the beginning of the Jenkyns Event at Peniche and Sogno, respectively.
452 Peti and Thibault (2017) linked *Schizosphaerella* sizes to paleotemperatures, namely large
453 valves produced under colder conditions and smaller valves prevailing under warm conditions. This
454 is reasonable for the general pattern observed also at Sogno, since the smallest average sizes correlates
455 with the Jenkyns Event hyperthermal as documented by $\delta^{18}O$ changes (Erba et al., 2022; Figure 5).
456 The comparison of morphometric data collected for schizosphaerellids at Sancerre (Peti and
457 Thibault. 2017), Peniche (Suan et al., 2010) and Sogno (this study) shows that in the Lombardy Basin
458 the valve sizes are ~2 μm smaller before, during and after the Jenkyns Event (Figure 12) than at the

459 other locations. Following Peti and Thibault (2017), such a shift might be related to the lower
460 paleolatitudes and presumably warmer temperatures in the Lombardy Basin during the Toarcian.
461 Mattioli and Pittet (2002) documented fluctuations of *Schizosphaerella* valve sizes across the
462 Upper Pliensbachian-Lower Toarcian Somma section in the Umbria-Marche Basin (Central Italy), at
463 a paleolatitude comparable (slightly lower) to the Sogno section. The average dimensions (between
464 the minimum and maximum diameter) is 1-1.5 µm larger at Somma relative to Sogno, suggesting
465 that paleotemperature was not the sole or dominant environmental factor affecting schizosphaerellid
466 valve sizes.
467 Numerous studies correlated the variations in size of several Mesozoic coccolith/nannolith
468 species with temperature (e.g. Bornemann and Mutterlose, 2006; Fraguas and Young, 2011; Ferreira
469 et al., 2017; Mattioli et al., 2004; Wulff et al., 2020; more references in Faucher et al., 2020). A size
470 difference comparable to the one identified in this study for *Schizosphaerella*, was documented for
471 *Biscutum constans* across OAE 2 (latest Cenomanian in age), with largest coccoliths observed at
472 higher latitudes (Faucher et al., 2017). However, the same pattern was not obtained for the early
473 Aptian OAE 1a, because *B. constans* showed similar coccolith sizes in the Tethys Ocean, at low
474 latitudes in the Pacific Ocean and in the Boreal Realm (Lübke et al., 2015; Faucher et al., 2017). A
475 causal link between size and temperature was disputed by Bottini and Faucher (2020) based on a ~28
476 million years long record of variations in *B. constans* coccolith size through the mid-Cretaceous.
477 Available paleotemperature proxies indicate that the smallest sizes correlate with cold temperatures,
478 but in general there isn't a relationship between coccolith dimensions and paleotemperatures (Bottini
479 and Faucher, 2020). Of course, *S. punctulata* does not belong to coccolithophores as does *B. constans*,
480 therefore the behavior of these two taxa may have been controlled by different ecological factors. The
481 comparison of our data with those from the Somma section (Mattioli and Pittet, 2002), indeed,
482 suggests that other factors (co)influenced the *S. punctulata* calcification.
483 The schizosphaerellid dimensional variations should be considered together with their
484 abundance to reconstruct the production of *Schizosphaerella* calcite and evaluate consequences for

pelagic biogenic carbonates. Mattioli and Pittet (2002) and Suan et al. (2008; 2010) quantified the schizospherellid contribution to carbonate deposition in the Umbria-Marche Basin and in the Lusitanian Basin, respectively, concluding that export from shallow-water carbonate platforms was much more relevant than calcareous nannoplankton production. Although quantitative data of *Schizosphaerella* calcite were derived applying different methodologies, previous estimates concur in concluding that schizosphaerellid calcite contribution was minor for hemipelagic and pelagic sedimentation, generally < 10% total calcium carbonate, without a significant correlation between schizosphaerellid $CaCO_3$ and bulk $CaCO_3$ when high-frequency lithological changes are concerned (Peti and Thibault, 2017). However, a broad co-variation was derived for longer-term changes and specifically across the Jenkyns Event (Peti and Thibault, 2017).

Fig.12: about here, full page width

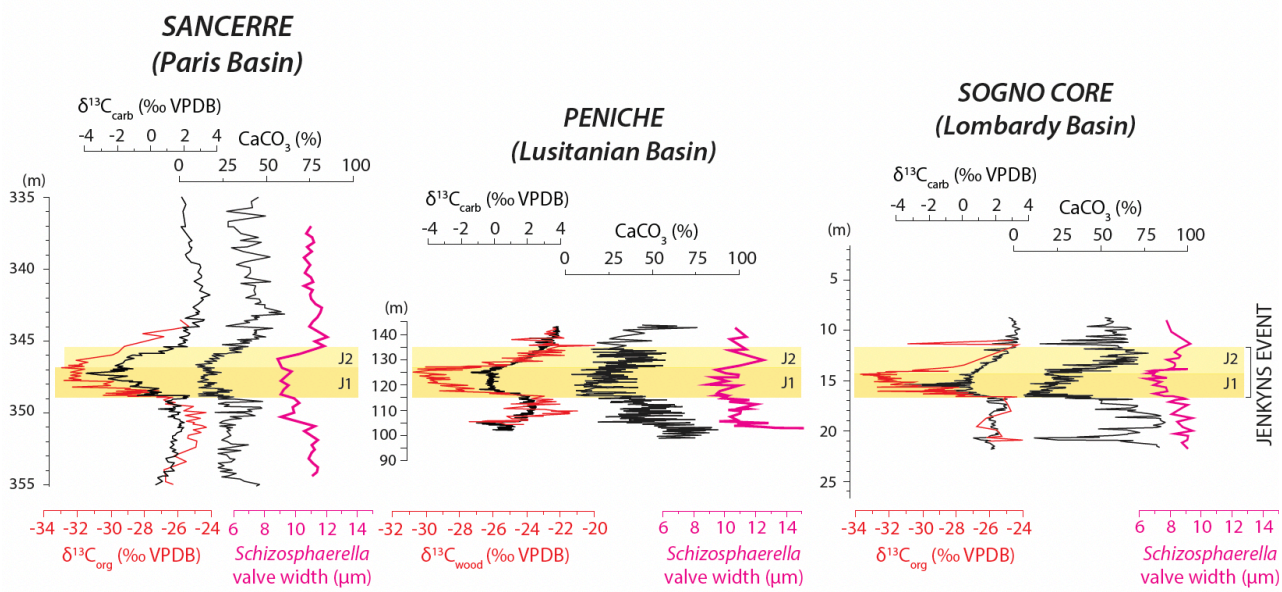

Figure 12. Comparison of $\delta^{13}C$, $CaCO_3$ and *Schizosphaerella* size variations at Sancerre borehole (Paris Basin, Clémence et al., 2015), Peniche section (Lusitanian Basin, Suan et al., 2008, 2010) and Sogno Core (Lombardy Basin, this study).

Our findings add interesting details for assessing the role of combined *Schizosphaerella* size and abundance in micrite production under a pelagic regime, with no shallow-water micrite contributions at Sogno. As discussed above, the separation of "small *S. punctulata*" (< 7 µm) abundance and size clearly indicates that there is a strong positive correlation between the absolute abundance and size of *S. punctulata* specimens > 7 µm and the $CaCO_3$ (Figure 10). However, such a

503 link is weakened by considering the entire *Schizosphaerella* cluster. Thus, we suspect that previous
504 conclusions are somehow influenced by potentially large amounts of small schizospaherellid
505 specimens, although we recognize that the hemipelagic nature of the sections examined in the Paris
506 and Lusitanian Basins was certainly prone to potentially receive considerable shallow-water micrite,
507 thus diluting the *Schizosphaerella* contribute to $CaCO_3$.

508 **4.2 Taxonomical implications**

509 The detailed investigations conducted by Kälin (1980) and Kälin and Bernoulli (1984) on
510 *Schizosphaerella* ultrastructure and diagenesis highlighted the formation of fringing radial calcite
511 during burial. The overgrowth of diagenetic crusts was reconducted to the crystal habit and
512 mineralogy of the skeletal elements and their mutual arrangement resulting in differential resistance
513 to early diagenesis. Based on a thorough characterization of ultrastructure details, Kälin and Bernoulli
514 (1984) concluded that only *S. punctulata* can develop a fringing crust of variable thickness whereas
515 such a diagenetic feature was not observed in *S. astraea* specimens. Indeed, the wall ultrastructure is
516 geometrically different supporting a diverse behavior of the two taxa during burial. In the lower part
517 of the Sogno Core we found *S. punctulata* and "encrusted *S. punctulata"* specimens together in the
518 same samples (both smear slides and thin sections) indicating that the same diagenetic
519 conditions/processes operated simultaneously producing species-specific effects.

520 The absence of "encrusted *S. punctulata"* in the black shale interval of the Fish Level might be
521 the result of different diagenetic conditions not producing radial calcite crusts. However, "encrusted
522 *S. punctulata"* specimens were not observed in the interval overlying the Fish Level consisting of
523 lithologies similar to those preceding the black shale interval and presumably with a similar
524 diagenetic history. Therefore, we conclude that the distribution of "encrusted *S. punctulata"* is not
525 entirely controlled by diagenesis and might reflect the occurrence of different *Schizosphaerella*
526 species.

Following Kälin and Bernoulli (1984), we conclude that possibly the *Schizosphaerella* specimens without diagenetic crusts belongs to *S. astraea* while encrusted specimens pertain to *S. punctulata*. This has important implications for taxonomy and, specifically for the separation of *S. punctulata* from *S. astraea* or their grouping within one taxon. *Schizosphaerella astraea* was established by Moshkovitz (1979) based on the ultrastructure pattern consisting of elongated crystallites radiating from a central knob and forming a star-like pattern and resulting in triangular pores. In *S. punctulata*, instead, single elements are arranged in a regular rectangular pattern and pores are rectangular in shape. Investigation of Lower Jurassic nannofossil assemblages using light and scanning electron microscopy have proved that only exceptionally well-preserved samples allow the identification of the original *Schizosphaerella* ultrastructure. Our record suggests that diagenesis might be diagnostic to distinguish the two *Schizosphaerella* species and suggests that *S. punctulata* was overwhelmed by *S. astraea* during the Jenkyns Event and the immediately following interval.

5. Conclusions

Absolute abundances and morphometric changes obtained for *S. punctulata* size-groups and "encrusted *S. punctulata*" (all specimens characterized by a crust surrounding the valve) revealed large fluctuations in the uppermost Pliensbachian–Lower Toarcian interval recovered with the Sogno Core. Relative to the onset and end of the T-OAE interval (Jenkyns, 1985, 1988, 2010), schizospharellids do not show changes in abundance or dimensions; both parameters record, instead, large fluctuations associated with the negative $\delta^{13}C$ Jenkyns Event. Specifically, the *Schizosphaerella* crisis interval initiated at the onset of the Jenkyns Event and its abundance recovery started in the earliest phase of the J2 segment. The schizosphaerellid abundance drop was essentially caused by the failure of *S. punctulata* specimens > 7 μm and "encrusted *S. punctulata*", while "small *S. punctulata*" (< 7 μm) maintained rather stable abundances through the investigated interval. The average valve dimension displays a 2 μm decreases in the *Schizosphaerella* crisis interval, but this size reduction

552 results from an abundance drop of specimens with valves > 7 μm. In fact, absolute abundances of
553 individual *S. punctulata* morphogroups unambiguously demonstrate that such a pattern is real and not
554 an artifact of relative abundances (closed sum problem). Thus, the average size decrease is not the
555 result of a general valve reduction, but rather derives from the decrease in relative abundance of
556 specimens > 7 μm.

557 As in the Sogno Core, a decrease in *Schizosphaerella* valve size across the Jenkyns Event was
558 documented for the Lusitanian and Paris basins, although the inception is diachronous while the
559 termination is synchronous based on high-resolution C-isotopic chemostratigraphy. It is worth
560 underlying that, although the reduction amplitude is analogous, there is a ~2 μm difference in size
561 between the schizosphaerellid average size from the Lombardy Basin relative to those from the
562 Lusitanian and Paris basins. At Sogno the average valve size is 1-1.5 μm smaller than in the Umbria
563 Marche-Basin. These data suggest that paleoenvironmental parameters (possibly ocean acidification
564 and fertility) other than – or in addition to – temperature probably affected, or at least co-controlled,
565 the nannofossil size.

566 The combined changes in *S. punctulata* abundance and size result in varying schizosphaerellid
567 calcite concurring to the deposition of micrite. The Sogno Core setting was pelagic with no evidence
568 of shallow-water carbonate debris, thus the micrite production should be proportional to plankton
569 biocalcification. Indeed, in the Sogno Core there is a strong positive correlation between the absolute
570 abundance and size of *S. punctulata* specimens > 7 μm and the $CaCO_3$ content, with a negligible
571 contribution to calcium carbonate by the "small *S.punctulata*" (< 7 μm) group. The concomitant drop
572 in abundance and shrinkage of valve average size across the *Schizosphaerella* crisis interval might be
573 a consequence of ocean acidification associated to excess CO_2 and global warming (Erba, 2004;
574 Tremolada et al., 2005; Mattioli et al., 2008; Casellato and Erba, 2015).

575 The co-occurrence in the same sample of *S. punctulata* specimens (> 7 μm) with and without a
576 crust is indicative of species-specific diagenetic effects. Based on the *S. punctulata* ultrastructure and
577 associated development of diagenetic features detailed by Kälin and Bernoulli (1984), we conclude

578 that specimens without diagenetic crusts belong to *S. astraea* while encrusted specimens are
579 attributable to *S. punctulata.* Within the "small *S. punctulata*" (< 7 μm) group no specimens with a
580 fringing crust were observed, suggesting that they all belong to *S. astraea*. We infer that the presence
581 of the diagenetic crust might be diagnostic to distinguish *S. punctulata* from *S. astraea,* the latter
582 becoming dominant during the Jenkyns Event and the following interval.
583
584 **Acknowledgments:**
585 This study profited from the very constructive reviews by E. Mattioli and an anonymous Reviewer.
586 We also thank the editor A. Dickson for his valuable suggestions on the manuscript. This research
587 was funded through PRIN 436 2017RX9XXXY awarded to EE and the Italian Ministry of Education
588 (MIUR) project "Dipartimenti di Eccellenza 753 2018–2022, Le Geoscienze per la Società: Risorse
589 e loro evoluzione.
590
591 **References**
592 Al-Suwaidi, A.H., Angelozzi, G.N., Baudin, F., Damborenea, S.E., Hesselbo, S.P., Jenkyns, H.C.,
593 Manceñido, M.O., Riccardi, A.C., 2010. First record of the early Toarcian Oceanic Anoxic
594 Event from the Southern Hemisphere, Neuquén Basin, Argentina. *J. Geol. Soc.*, *167*, 633–
595 636, https://doi.org/10.1144/0016-76492010-025
596 Bottini, C., Faucher, G., 2020. *Biscutum constans* coccolith size patterns across the mid Cretaceous
597 in the western Tethys: Paleoecological implications. *Palaeogeogr. Palaeoclimatol.*
598 *Palaeoecol.*, *555*, 109852. https://doi.org/10.1016/j.palaeo.2020.109852
599 Bornemann, A., Mutterlose, J., 2006. Size analyses of the coccolith species Biscutum constans and
600 Watznaueria barnesiae from the Late Albian "Niveau Breistroffer"(SE France): taxonomic
601 and palaeoecological implications. *Geobios*, 39(5), 599-615,
602 https://doi.org/10.1016/j.geobios.2005.05.005.
603 Bown, P.R., 1987. Taxonomy, evolution, and biostratigraphy of late Triassic-early Jurassic
604 calcareous nannofossils. *Palaeontol. Ass., spec. pap. palaeontol., 32*, 118 pp.
605 Bown, P., 1998. Calcareous nannofossil biostratigraphy (pp. 1-315). *Chapman and Hall; Kluwer*
606 *Academic.*

607 Bown, P.R., Lees, J.A., Young, J.R., 2004. Calcareous nannoplankton evolution and diversity through
608 time. In *Coccolithophores: from molecular processes to global impact*, Thierstein, H.R.,
609 Young J.R., Eds., Springer, Berlin, Heidelberg, pp. 481–508.

610 Bucefalo Palliani, R. B., Mattioli, E., Riding, J. B, 2002. The response of marine phytoplankton and
611 sedimentary organic matter to the early Toarcian (Lower Jurassic) oceanic anoxic event in
612 northern England. *Mar. micropaleontol.*, *46.3-4*, 223–245, https://doi.org/10.1016/S0377-
613 8398(02)00064-6.

614 Caruthers, A.H., Gröcke, D.R., Smith, P.L., 2011. The significance of an early Jurassic (Toarcian)
615 carbon-isotope excursion in Haida Gwaii (Queen Charlotte Islands), British Columbia,
616 Canada. *Earth Planet. Sci. Lett.*, *307*, 19–26, https://doi.org/10.1016/j.epsl.2011.04.013.

617 Casellato, C.E., Erba, E., 2015. Calcareous nannofossil biostratigraphy and paleoceanography of the
618 Toarcian Oceanic Anoxic event at Colle di Sogno (southern Alps, northern Italy). *Riv. Ital. di*
619 *Paleontol. e Stratigr.*, *121.3*, 297–327.

620 Channell, J.E.T., Casellato, C.E., Muttoni, G., Erba, E., 2010. Magnetostratigraphy, nannofossil
621 stratigraphy and apparent polar wander for Adria-Africa in the Jurassic–Cretaceous boundary
622 interval. *Palaeogeogr. Palaeoclimatol. Palaeoecol.*, *293*, 51–75,
623 https://doi.org/10.1016/j.palaeo.2010.04.030.

624 Claps, M., Erba, E., Masetti, D., Melchiorri, 1995. F. Milankovitch-type cycles recorded in Toarcian
625 black shales from Belluno Through (Southern Alps, Italy). *Mem. Soc. Geol. Ital.* 1995, *47*, 179–
626 188.

627 Clémence, M.E., Gardin, S., Bartolini, 2015. A. New insights in the pattern and timing of the early
628 Jurassic calcareous nannofossil crisis. *Palaeogeogr. Palaeoclimatol. Palaeoecol.*, *427*, 100–
629 108, https://doi.org/10.1016/j.palaeo.2015.03.024

630 Cobianchi, M., 1992. Sinemurian - early Bajocian calcareous nannofossil biostratigraphy of the
631 Lombardian Basin (Southern calcareous Alps; Northen Italy). *Atti ticinensi Sci. terra*, *35*, 61–
632 106.

633 Dal Piaz, G.V., 1907. Le Alpi feltrine: studio geologico. *Mem. R. Ist. Veneto Sci. Lett. Arti*, 27.9, 176
634 pp.

635 Deflandre, G., Dangeard, L., 1938. Schizosphaerelle, un nouveau microfossile méconnu du jurassique
636 moyen et supérieur. *C. R. Acad. Sci. Paris*, *207*, 1115–1117.

637 Demangel, I., Kovács, Z., Richoz, S., Gardin, S., Krystyn, L., Baldermann, A., Piller, W. E., 2020.
638 Development of early calcareous nannoplankton in the late Triassic (Northern Calcareous
639 Alps, Austria). *Global Planet change*, *193*, 103254.

https://doi.org/10.1016/j.gloplacha.2020.103254

Emmanuel, L., Renard, M., Cubaynes, R., De Rafelis, M., Hermoso, M., Lecallonnec, L., Le Solleuz, A., Rey, J., 2006. The "Schistes Carton" of Quercy (Tarn, France): a lithological signature of a methane hydrate dissociation event in the early Toarcian. Implications for correlations between Boreal and Tethyan realms. *Bull. Soc. Géol. Fr.*, *177*, 239–249.

Erba, E., 2004. Calcareous nannofossils and Mesozoic oceanic anoxic events. *Mar. Micropaleontol.*, *52*, 85–106, https://doi.org/10.1016/j.marmicro.2004.04.007.

Erba, E., 2006. The first 150 million years history of calcareous nannoplankton: Biosphere – Geosphere interaction. *Palaeogeogr. Palaeoclimatol. Palaeoecol.*, *232*, 237–250, https://doi.org/10.1016/j.palaeo.2005.09.013.

Erba, E., Tremolada, F., 2004. Nannofossil carbonate fluxes during the early Cretaceous: Phytoplankton response to nutrification episodes, atmospheric CO_2, and anoxia. *Paleoceanography*, *19*.1. https://doi.org/10.1029/2003PA000884

Erba, E., Bottini, C., Faucher, G., Gambacorta, G., Visentin, S., 2019a. The response of calcareous nannoplankton to Oceanic Anoxic Events: the Italian pelagic record. *Boll. Soc. Paleontol. Ital., 58.1*, 51–71.

Erba, E., Gambacorta, G., Visentin, S., Cavalheiro, L., Reolon, D., Faucher, G., Pegoraro, M., 2019b. Coring the sedimentary expression of the early Toarcian Oceanic Anoxic Event: new stratigraphic records from the Tethys Ocean. *Sci. Drill.*, *26*, 17–27, https://doi.org/10.5194/sd-26-17-2019.

Erba, E., Cavalheiro, L., Dickson, A.J., Faucher, G., Gambacorta, G., Jenkyns, H.C., Wagner, T., 2022. Carbon- and oxygen-isotope signature of the Toarcian Oceanic Anoxic Event: insights from two Tethyan pelagic sequences (Gajum and Sogno Cores - Lombardy Basin, norther Italy). *Newsl. Stratigr*. (published OnLine) DOI: 10.1127/nos/2022/0690.

Fantasia, A. Föllmi, K.B. Adatte, T., Bernaìrdez, E., Spangenberg, J.E., Mattioli, E., 2018. The Toarcian Oceanic Anoxic Event in southwestern Gondwana: an example from the Andean Basin, northern Chile. *J. Geol. Soc.*, *175*, 883–902.

Faucher, G., Erba, E., Bottini, C., Gambacorta, G., 2017. Calcareous nannoplankton response to the latest Cenomanian Oceanic Anoxic Event 2 perturbation. *Riv. Ital. di Paleontol. e Stratigr*., *123*, 159–176.

Faucher, G., Riebesell, U., Bach, L. T., 2020. Can morphological features of coccolithophores serve as a reliable proxy to reconstruct environmental conditions of the past?. *Climate of the Past*, 16(3), 1007-1025 https://doi.org/10.5194/cp-16-1007-2020.

Ferreira, J., Mattioli, E., van de Schootbrugge, B., 2017. Palaeoenvironmental vs. evolutionary

674 control on size variation of coccoliths across the Lower-Middle Jurassic. *Palaeogeography,*
675 *Palaeoclimatology, Palaeoecology,* 465, 177-192,
676 https://doi.org/10.1016/j.palaeo.2016.10.029.
677 Filatova, N.I., Konstantinovskaya, E., Vishnevskaya, V., 2020. Jurassic–Lower Cretaceous siliceous
678 rocks and black shales from allochthonous complexes of the Koryak-Western Kamchatka
679 orogenic belt, East Asia. *Int. Geol. Rev.*, 1–20.
680 Fraguas, Á., Comas-Rengifo, M.J., Gomez, J.J., Goy, A., 2012. The calcareous nannofossil crisis in
681 Northen Spain (Asturias province) linked to the early Toarcian warming-driven mass
682 estinction. *Mar. Micropalentol.*, *94-95*, 58–71,
683 https://doi.org/10.1016/j.marmicro.2012.06.004
684 Fraguas, Á., Gómez, J. J., Goy, A., Comas-Rengifo, M. J., 2021. The response of calcareous
685 nannoplankton to the latest Pliensbachian–early Toarcian environmental changes in the
686 Camino Section (Basque Cantabrian Basin, northern Spain). *Geological Society, London,*
687 *Special Publications*, 514(1), 31-58, https://doi.org/10.1144/SP514-2020-256
688 Fraguas, Á., Young, J. R., 2011. Evolution of the coccolith genus Lotharingius during the Late
689 Pliensbachian-Early Toarcian interval in Asturias (N Spain). Consequences of the Early
690 Toarcian environmental perturbations. *Geobios*, 44(4), 361-375,
691 https://doi.org/10.1016/j.geobios.2010.10.005.
692 Gaetani, M., Poliani, G., 1978. Il Toarciano e il Giurassico medio in Albenza (Bergamo). *Riv. Ital. di*
693 *Paleontol. e Stratigr.*, *84*, 349–382.
694 Gaetani, M., Erba, E., 1990. Il bacino Lombardo: un sistema paleoalto/fossa in un margine
695 continentale passivo durante il Giurassico. 75° Congresso Società Geologica Italiana, Guida
696 all'escursione A3, Milano, Italy. 10–12 September.
697 Gardin, S., Krystyn, L., Richoz, S., Bartolini, A., Galbrun, B., 2012. Where and when the earliest
698 coccolithophores?. *Lethaia*, 45(4), 507-523, https://doi.org/10.1111/j.1502-
699 3931.2012.00311.x
700 Geisen M.; Bollmann J., Herrle J.O., Mutterlose J., Youg J. R., 1999. Calibration of the random
701 settling technique for calculation of absolute abundances of calcareous nannoplankton.
702 *Micropaleontology*, *45*, 437–442,
703 Gröcke, D.R., Hori, R.S., Trabucho-Alexandre, J., Kemp, D.B., Schwark, L., 2011. An open ocean
704 record of the Toarcian oceanic anoxic event. *Solid Earth*, *2*, 245–257,
705 https://doi.org/10.5194/se-2-245-2011.
706 Hermoso, M., Le Callonnec, L., Minoletti, F., Renard, M., Hesselbo, S.P., 2009. Expression of the
707 early Toarcian negative carbon-isotope excursion in separated carbonate microfractions

(Jurassic, Paris Basin). *Earth Planet. Sci. Lett.*, *277.1-2*, 194–203, https://doi.org/10.1016/j.epsl.2008.10.013.

Hermoso, M., Minoletti, F., Rickaby, R.E.M., Hesselbo, S.P., Baudin, F., Jenkyns, H.C., 2012. Dynamics of a stepped carbon-isotope excursion: Ultra high-resolution study of early Toarcian environmental change. *Earth Planet. Sci. Lett.*, *319-320*, 45–54, https://doi.org/10.1016/j.epsl.2011.12.021.

Hesselbo, S.P., Gröcke, D.R., Jenkyns, H.C., Bjerrum, C.J., Farrimond, P., Morgans Bell, H.S.; Green, O.R., 2000. Massive dissociation of gas hydrate during a Jurassic Oceanic Anoxic Event. *Nature*, *406*, 392–395, https://doi.org/10.1038/35019044

Hesselbo, S.P., Jenkyns, H.C., Duarte, L.V., Oliveira, L.C.V., 2007. Carbon-isotope record of the early Jurassic (Toarcian) Oceanic Anoxic Event from fossil wood and marine carbonate (Lusitanian Basin, Portugal). *Earth Planet. Sci. Lett.*, *253*, 455–470, https://doi.org/10.1016/j.epsl.2006.11.009

Hesselbo, S.P., Pieńkowski, G., 2011. Stepwise atmospheric carbon-isotope excursion during the Toarcian Oceanic Anoxic Event (early Jurassic, Polish Basin). *Earth Planet. Sci. Lett.*, *301*, 365–372, https://doi.org/10.1016/j.epsl.2010.11.021.

Hinnov, L.A, Park, J. Erba, E., 2000. Lower-Middle Jurassic rhythmites from the Lombard Basin, Italy: a record of orbitally forced carbonate cycles modulated by secular environmental changes in West Tethys. In *Advances in Jurassic Research*; Hall, R.L., Smith, P.L., Eds.; Trans Tech Publications, Zurich, Switzerland, pp. 437–454.

Hougård, I.W., Bojese-Koefoed, J.A., Vickers, M.L., Ullmann, C.V., Bjerrum, C.J., Rizzi, M., Korte, C., 2021. Redox element record shows that environmental perturbations associated with the T-OAE were of longer duration than the carbon isotope record suggests – the Aubach section, SW Germany. *Newsl. Stratigr.*, *54.2*, 229–246.

Ikeda, M., Hori, R.S., Ikehara, M., Miyashita R., Chino, M., Yamada. K., 2018. Carbon cycle dynamics linked with Karoo-Ferrar volcanism and astronomical cycles during Pliensbachian-Toarcian (early Jurassic). *Global Planet. Change*, *170*, 163–171, https://doi.org/10.1016/j.gloplacha.2018.08.012

Izumi, K., Miyaji, T., Tanabe, K., 2012. early Toarcian (early Jurassic) oceanic anoxic event recorded in the shelf deposits in the northwestern Panthalassa: evidence from the Nishinakayama formation in the Toyora area, west Japan. *Palaeogeogr. Palaeoclimatol. Palaeoecol.*, *315-316*, 100–108, https://doi.org/10.1016/j.palaeo.2011.11.016.

Jenkyns, H.C., 1985. The early Toarcian and Cenomanian-Turonian anoxic events in Europe: comparisons and contrasts. *Geol. Rundsch.*, *74*, 505–518.

742 Jenkyns, H.C., 1988. The early Toarcian (Jurassic) Anoxic Event: stratigraphic, sedimentary and
743 geochemical evidence. *Am. J. Sci.*, *288*, 101–151.
744 Jenkyns, H.C., 2003. Evidence for rapid climate change in the Mesozoic–Palaeogene greenhouse
745 world. *Philos. Trans. R. Soc. Lond., A*, *361*, 1885–1916.
746 Jenkyns, H.C., 2010. Geochemistry of oceanic anoxic events. *Geochem. Geophys. Geosyst.*, *11.3*, 1–
747 30. https://doi.org/10.1029/2009GC002788
748 Jenkyns, H.C., Clayton, C.J., 1986 Black shales and carbon isotopes in pelagic sediments from the
749 Tethyan Lower Jurassic. *Sedimentology*, *33*, 87–106.
750 Jenkyns, H.C., Clayton, C.J., 1997. Lower Jurassic epicontinental carbonates and mudstones from
751 England and Wales: chemostratigraphic signals and the early Toarcian anoxic event.
752 *Sedimentology*, *44*, 687–706.
753 Jenkyns, H.C., Gröcke, D.R., Hesselbo, S.P., 2001. Nitrogen isotope evidence for water mass
754 denitrification during the early Toarcian (Jurassic) oceanic anoxic event. *Paleoceanography*,
755 *16*, 593–603, https://doi.org/10.1029/2000PA000558
756 Jenkyns, H.C., Jones, C.E., Gröcke, D.R., Hesselbo, S.P., Parkinson, D.N., 2002. Chemostratigraphy
757 of the Jurassic System: applications, limitations and implications for palaeocenography. *J.*
758 *Geol. Soc.*, *159*, 351–378, https://doi.org/10.1144/0016-764901-130.
759 Kafousia, N., Karakitsios, V., Jenkyns, H.C., Mattioli, E., 2011. A global event with a regional
760 character: the early Toarcian Oceanic Anoxic Event in the Pindos Ocean (northern
761 Peloponnese, Greece). *Geol. Mag.*, *148*, 619–631.
762 Kafousia, N., Karakitsios, V., Mattioli, E., Kenjo, S., Jenkyns H.C., 2014. The Toarcian Oceanic
763 Anoxic Event in the Ionian Zone, Greece. *Palaeogeogr. Palaeoclimatol. Palaeoecol.*, *393*,
764 135–145, https://doi.org/10.1016/j.palaeo.2013.11.013.
765 Kälin, O., 1980. *Schizosphaerella punctulata* Deflandre & Dangeard: wall ultrastructure and
766 preservation in deep-water carbonate sediments of the Tethyan Jurassic. *Eclogae Geol. Helv.*,
767 *73.3*, 983–1008.
768 Kälin, O., Bernoulli, D., 1984. *Schizosphaerella* Deflandre & Dangeard in Jurassic deeper-water
769 carbonate sediments, Mazagan Continental Margin (Hole 547B) and Mesozoic Tethys. *Initial*
770 *Reports DSDP*, *79*, 411–429.
771 Kemp, D.B., Coe, A.L., Cohen, A.S., Schwark, L., 2005. Astronomical pacing of methane release in
772 the early Jurassic period. *Nature*, *437*, 396–399, https://doi.org/10.1038/nature04037.
773 Lübke, N., Mutterlose, J., Bottini, C., 2015. Size variations of coccoliths in Cretaceous oceans—A
774 result of preservation, genetics and ecology?. *Marine Micropaleontology*, 117, 25-39,
775 https://doi.org/10.1016/j.marmicro.2015.03.002.

776 Mattioli, E., 1997. Nannoplankton productivity and diagenesis in the rhythmically bedded Toarcian-
777 Aalenian Fiuminata section (Umbria-Marche Apennine, central Italy). *Palaeogeogr.*
778 *Palaeoclimatol. Palaeoecol.*, *130.1-4*, 113–133, https://doi.org/10.1016/S0031-
779 0182(96)00127-7

780 Mattioli, E., Erba E., 1999. Synthesis of calcareous nannofossil events in Tethyan Lower and Middle
781 Jurassic successions. *Riv. Ital. di Paleontol. e Stratigr.*, *105.3*. https://doi.org/10.13130/2039-
782 4942/5380

783 Mattioli, E., Pittet, B., 2002. Contribution of calcareous nannoplankton to carbonate deposition: a
784 new approach applied to the Lower Jurassic of Central Italy. *Mar. Micropaleontol.*, *45*, 175–
785 190, https://doi.org/10.1016/S0377-8398(02)00039-7.

786 Mattioli, E., Pittet, B., Palliani, R., Röhl, H. J., Schmid-Röhl, A., Morettini, E., 2004. Phytoplankton
787 evidence for the timing and correlation of palaeoceanographical changes during the early
788 Toarcian oceanic anoxic event (early Jurassic). *J. Geol. Soc.*, *161.4*, 685–693.

789 Mattioli, E., Pittet, B., Suan, G., Mailliot, S., 2008. Calcareous nannoplankton changes across the
790 early Toarcian oceanic anoxic event in the western Tethys. *Paleoceanography*, *23*, 1–17,
791 https://doi.org/10.1029/2007PA001435

792 Mattioli, E., Pittet, B., Petipierre, L., Mailliot, S., 2009. Dramatic decrease of pelagic carbonate
793 production by nannoplankton across the early Toarcian anoxic event (T-OAE). *Global Planet.*
794 *Change*, *65*, 134-145. https://doi.org/10.1016/j.gloplacha.2008.10.018

795 McElwain, J.C., Wade-Murphy, J., Hesselbo, S.P., 2002. Changes in carbon dioxide during an
796 oceanic anoxic event linked to intrusion into Gondwana coals. *Nature, 435*, 479–482,
797 https://doi.org/10.1038/nature03618

798 Menini, A., Mattioli, E., Hesselbo, S. P., Ruhl, M., Suan, G., 2021. Primary versus carbonate
799 production in the Toarcian, a case study from the Llanbedr borehole (Mochras Farm,
800 Wales). *Geol. Soc. Spec. Publ.*, *514*. https://doi.org/10.1144/SP514-2021-19

801 Moshkovitz, S., 1979. On the distribution of *Schizophaerella punctulata* Deflandre & Dangeard and
802 *Schizosphaerella astraea* n.sp. in the Liassic section of Stowell Park Borehole
803 (Gloucestershire) and in some other Jurassic localities in England. *Eclogae Geol. Helv*., *72*,
804 455–465.

805 Müller, T., Price, G.D., Bajnai, D., Nyerges, A., Kesjár, D., Raucsik, B., Varga, A., Judik, K., Fekete,
806 J., May, Z., and Pálfy, J., 2017. New multiproxy record of the Jenkyns Event (also known as
807 the Toarcian OceanicAnoxic Event) from the Mecsek Mountains (Hungary): Differences,
808 duration and drivers. *Sedimentology*, *64*, 66–86, https://doi.org/10.1111/sed.12332.

Müller, T., Jurikova, H., Gutjahr, M., Tomašových, A., Schlögl, J., Liebetrau, V., Duarte, L.V., Milovsky, R., Suan, G., Mattioli, E., Pittet, B., Eisenhauer, A., 2020. Ocean acidification during the early Toarcian extinction event: Evidence from boron isotopes in brachiopods. *Geology*, *48.12*, 1184–1188, https://doi.org/10.1130/G47781.1

Muttoni, G., Erba, E., Kent, D.V., Bachtadse, V., 2005. Mesozoic Alpine facies deposition as a result of past latitudinal plate motion. *Nature*, *434*, 59–63, https://doi.org/10.1038/nature03378.

Peti, L., Thibault, N., 2017. Abundance and size changes in the calcareous nannofossil *Schizosphaerella* - Relation to sea-level, the carbonate factory and palaeoenvironmental change from the Sinemurian to earliest Toarcian of the Paris Basin. *Palaeogeogr. Palaeoclimatol. Palaeoecol.*, *485*, 271–282 https://doi.org/10.1016/j.palaeo.2017.06.019.

Peti, L., Thibault, N., Korte, C., Ullmann, C. V., Cachão, M., Fibæk, M., 2021. Environmental drivers of size changes in Lower Jurassic *Schizosphaerella* spp. *Mar. Micropaleontol.*, 102053. https://doi.org/10.1016/j.marmicro.2021.102053

Remirez, M.N., Algeo, T.J., 2020. Carbon-cycle changes during the Toarcian (early Jurassic) and implications for regional versus global drivers of the Toarcian oceanic anoxic event. *Earth Sci. Rev.*, *209*, 103283. https://doi.org/10.1016/j.earscirev.2020.103283

Reolid, M., Mattioli, E., Nieto, L.M., Rodriguez-Tovar, F.J., 2014. The early Toarcian Oceanic Anoxic Event in the External Subbetic (Southiberian Paleomargin, Westernmost Tethys): geochemistry, nannofossils and ichnology. *Palaeogeogr. Palaeoclimatol. Palaeoecol.*, *411*, 79–94, https://doi.org/10.1016/j.palaeo.2014.06.023.

Reolid, M., Mattioli, E., Duarte, L. V., Marok, A., 2020. The Toarcian Oceanic Anoxic Event and the Jenkyns Event (IGCP-655 final report). *Episodes*, *43.2*, 833–844.

Röhl, H.-J., Schmid-Röhl, A., Oschmann, W., Frimmel, A., Schwark, L., 2001. The Posidonia Shale (Lower Toarcian) of SW-Germany: an oxygen-depleted ecosystem controlled by sea level and palaeoclimate. *Palaeogeogr. Palaeoclimatol. Palaeoecol.*, *165*, 27–52, https://doi.org/10.1016/S0031-0182(00)00152-8.

Ruebsam, W., Müller, T., Kovács, J., Pálfy, J., Schwark, L., 2018. Environmental response to the early Toarcian carbon cycle and climate perturbations in the northeastern part of the West Tethys shelf. *Gondwana Res.*, *59*, 144–158, https://doi.org/10.1016/j.gr.2018.03.013.

Ruebsam, W., Al-Husseini, M., 2020. Calibrating the early Toarcian (early Jurassic) with stratigraphic black holes (SBH). *Gondwana Res.*, *82*, 317–336, https://doi.org/10.1016/j.gr.2020.01.011.

Sabatino, N., Neri, R., Bellanca, A., Jenkyns, H.C., Baudin, F., Parisi, G., Masetti, D., 2009. Carbon-isotope records of the early Jurassic (Toarcian) oceanic anoxic event from the Valdorbia

(Umbria-Marche Apennines) and Monte Mangart (Julian Alps) sections: palaeoceanographic and stratigraphic implications. *Sedimentology*, *56*, 1307–1328, https://doi.org/10.1111/j.1365-3091.2008.01035.x.

Schouten, S., van Kaam-Peters, H.M.E., Rijpstra,W.I.C., Schoell, M., Sinninghe Damsté, J.S., 2000. Effects of an oceanic anoxic event on the stable carbon isotopic composition of early Toarcian carbon. *Am. J. Sci.*, *300*, 1–22, https://doi.org/10.2475/ajs.300.1.1.

Suan, G., Pittet, B., Bour, I., Mattioli, E., Duarte, L.V., Mailliot, S., 2008. Duration of the Early Toarcian carbon isotope excursion deduced from spectral analysis: Consequence for its possible causes. *Earth Planet. Sci. Lett.*, *267*, 666–679, https://doi.org/10.1016/j.epsl.2007.12.017.

Suan, G., Mattioli, E., Pittet, B., Lécuyer, C., Suchéras-Marx, B., Duarte, L.V., Philippe, M., Reggiani, L., Martineau, F., 2010. Secular environmental precursors to early Toarcian (Jurassic) extreme climate changes. *Earth Planet Sci. Lett.*, *290*, 448–458, https://doi.org/10.1016/j.epsl.2009.12.047.

Them, T.R., Gill, B.C., Selby, D., Gröcke, D.R., Friedman, R.M., Owens, J.D., 2017. Evidence for rapid weathering response to climatic warming during the Toarcian Oceanic Anoxic Event. *Sci. Rep.*, *7.1*, 1–10, https://doi.org/10.1038/s41598-017-05307-y

Trabucho-Alexandre, J., Dirkx, R., Veld, H., Klaver, G., De Boer, P., 2012. Toarcian black shales in the Dutch Central Graben: record of energetic, variable depositional conditions during an oceanic anoxic event. *J. Sedimen. Res.*, *82*, 104–120, https://doi.org/10.2110/jsr.2012.5.

Tremolada, F., van de Schootbrugge, B.V., Erba, E., 2005. Early Jurassic schizosphaerellid crisis in Cantabria, Spain: implications for calcification rates and phytoplankton evolution across the Toarcian oceanic anoxic event. *Paleoceanography*, *20*, 1–11, https://doi.org/10.1029/2004PA00112.

van Breugel, Y. Baas, M. Schouten, S. Mattioli, E. Damsté, J.S.S., 2006. Isorenieratane record in black shales from the Paris Basin, France: Constraints on recycling of respired CO_2 as a mechanism for negative carbon isotope shifts during the Toarcian oceanic anoxic event. *Paleoceanography*, *21.4*, 1–8, https://doi.org/10.1029/2006PA001305.

Visentin, S., Erba, E., 2021. High-resolution calcareous nannofossil biostratigraphy across the Toarcian Oceanic Anoxic Event in northern Italy: clues from the Sogno and Gajum Cores (Lombardy Basin, Southern Alps). *Riv. Ital. di Paleontol. e Stratigr.*, *127*, 539–556.

Visentin, S., Erba, E., Mutterlose, J., 2021. Bio- and chemostratigraphy of the Posidonia Shale: a new database for the Toarcian Anoxic Event from northern Germany. *Newsl. Stratigr.* https://doi.org/10.1127/nos/2021/0658

Wulff, L., Mutterlose, J., Bornemann, A., 2020. Size variations and abundance patterns of calcareous nannofossils in mid Barremian black shales of the Boreal Realm (Lower Saxony Basin). *Marine Micropaleontology*, 156, 101853, https://doi.org/10.1016/j.marmicro.2020.101853.

Xu, W., Ruhl, M., Jenkyns, H.C., Hesselbo, S.P. Riding, J.B., Selby, D., Naafs, B.D.A., Weijers, J.W.H. Pancost, R.D., Tegelaar, E., Idiz, E., 2017. Carbon sequestration in an expanded lake system during the Toarcian oceanic anoxic event. *Nat. Geosci.*, *10*, 129–134, https://doi.org/10.1038/ngeo2871.